The effect of model tidal forcing on virtual particle dispersion and accumulation at the ocean surface

Laura Gomez-Navarro[1,1], Erik Van Sebille[1,1], Verónica MORALES MÁRQUEZ[2,2], Ismael Hernandez-Carrasco[3,3], Aurelie Albert[4,4], Clement Ubelmann[5,5], Julien Le Sommer[6,6], Jean-Marc Molines[7,7], and Laurent Brodeau[5,5]

[1]Utrecht University
[2]Institut Méditerranéen d'Océanologie
[3]SOCIB / IMEDEA
[4]Universite Grenoble Alpes /CNRS/IGE
[5]Datlas
[6]Univ. Grenoble Alpes, CNRS, IRD, Grenoble INP, IGE
[7]French National Centre for Scientific Research (CNRS)

December 7, 2023

Abstract

Understanding the pathways of floating material at the surface ocean is important to improve our knowledge on surface circulation and for its ecological and environmental impacts. Virtual particle simulations are a common method to simulate the dispersion of floating material. To advect the particles, ocean models' velocities are usually used, but only recent ones include tidal forcing. Our research question is: What is the effect of tidal forcing on virtual particle dispersion and accumulation at the ocean surface? As inputs we use velocity outputs from eNATL60, a twin simulation with and without tidal forcing. We focus on the Açores Islands region and we find: 1) Surface particles have a larger displacement, but a lower distance travelled with than without tidal forcing 2) Surface accumulation seasonal differences depend on the spatial scale of the ocean structures 3) A greater variability in surface accumulation is present with tidal forcing.

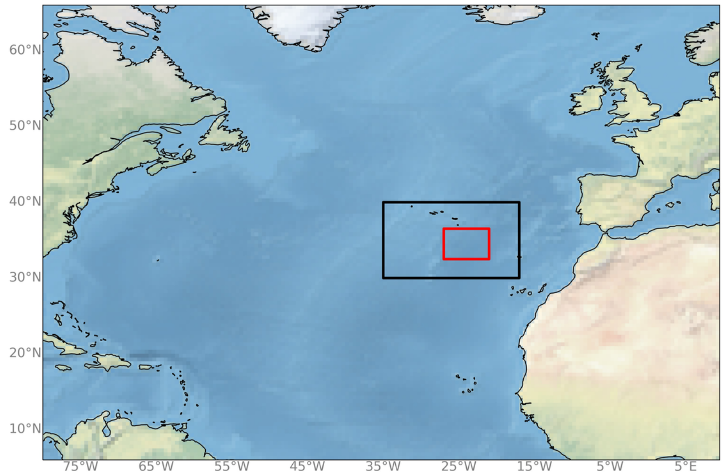

Figure 1: Spatial domain of the eNATL60 simulation (except the Gulf of Mexico, Black Sea and eastern Mediterranean Sea domains). Black box shows the region of this study where virtual surface particles are released. Red box shows the subregion used for some of the analyses.

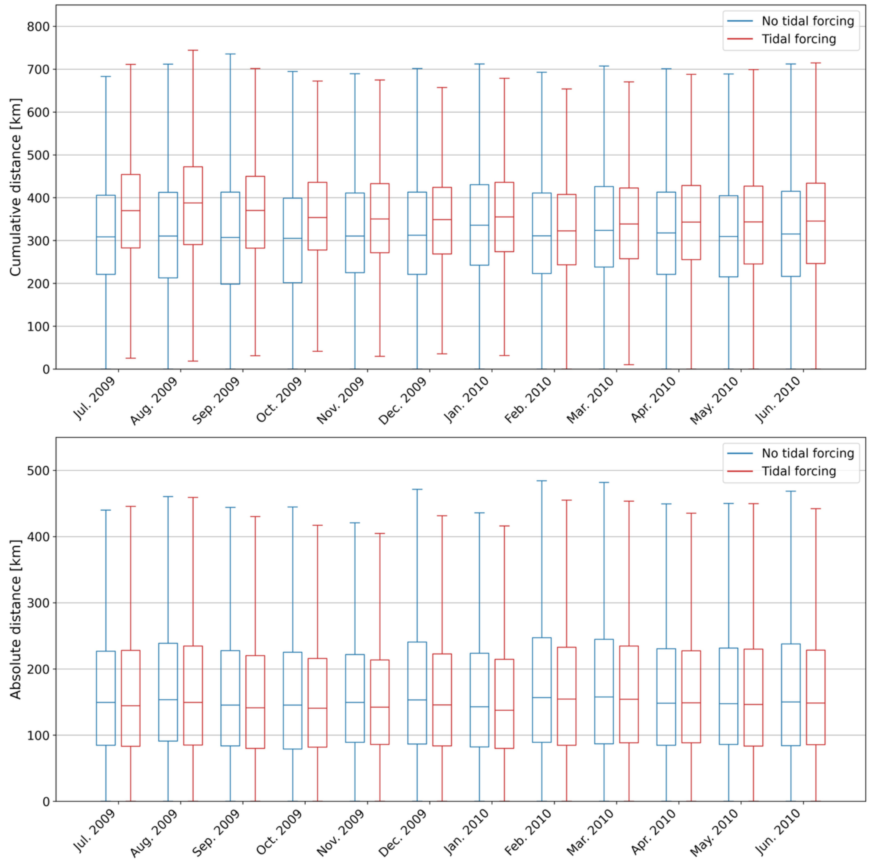

Figure 2: Box plots of mean cumulative distance [km] (top) and mean absolute distance [km] (bottom) travelled by the virtual particles per month.

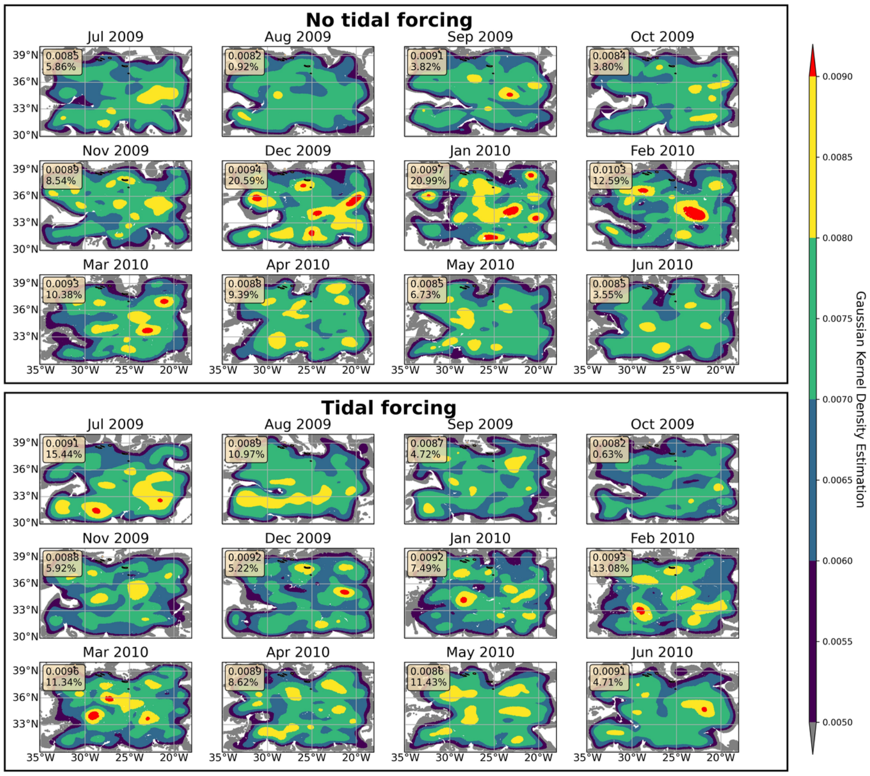

Figure 3: Gaussian Kernel Density Estimation (GKDE) comparison between non-tidal (top) and tidal (bottom) simulations. Maximum GKDE value (top) and percentage of particles with a high GKDE value (greater than 0.008) (bottom) are shown in the bottom left textbox.

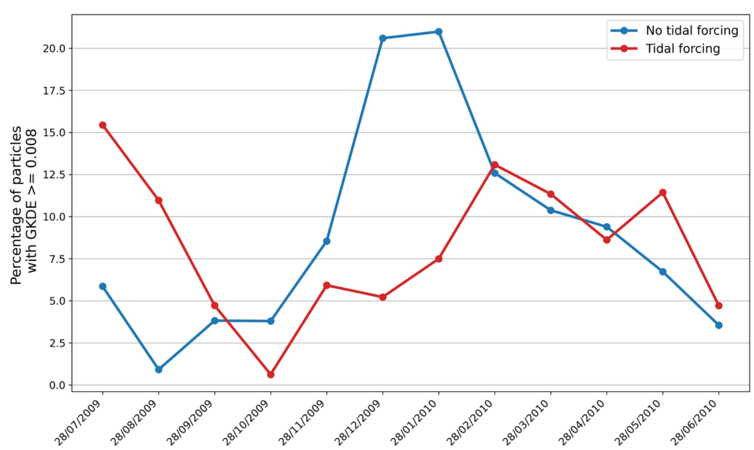

Figure 4: Comparison of the percentage of particles with a high GKDE value (greater than 0.008) per month. Non-tidal results are shown in blue and tidal in red.

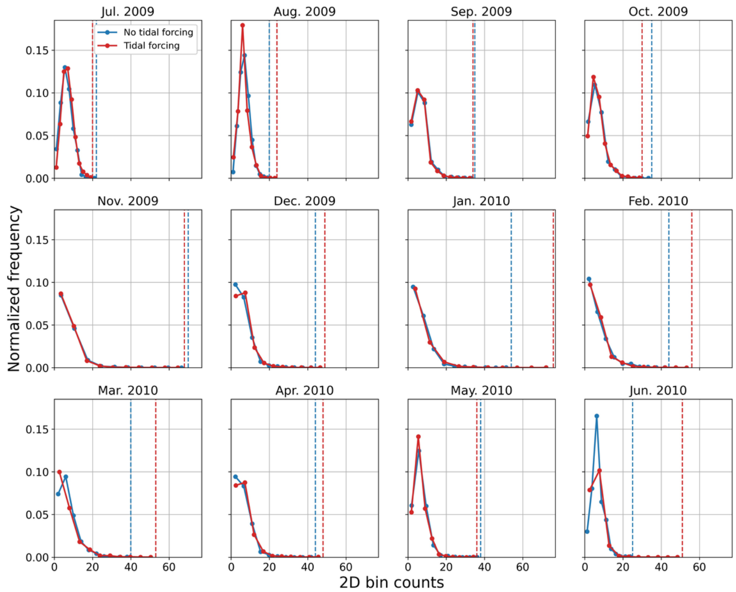

Figure 5: 1D histogram of the 2D histogram of the distribution of the particles after 28 days of advection. Results of the non-tidal simulation are shown in blue and from the tidal in red. Vertical, dashed lines indicate the maximum value.

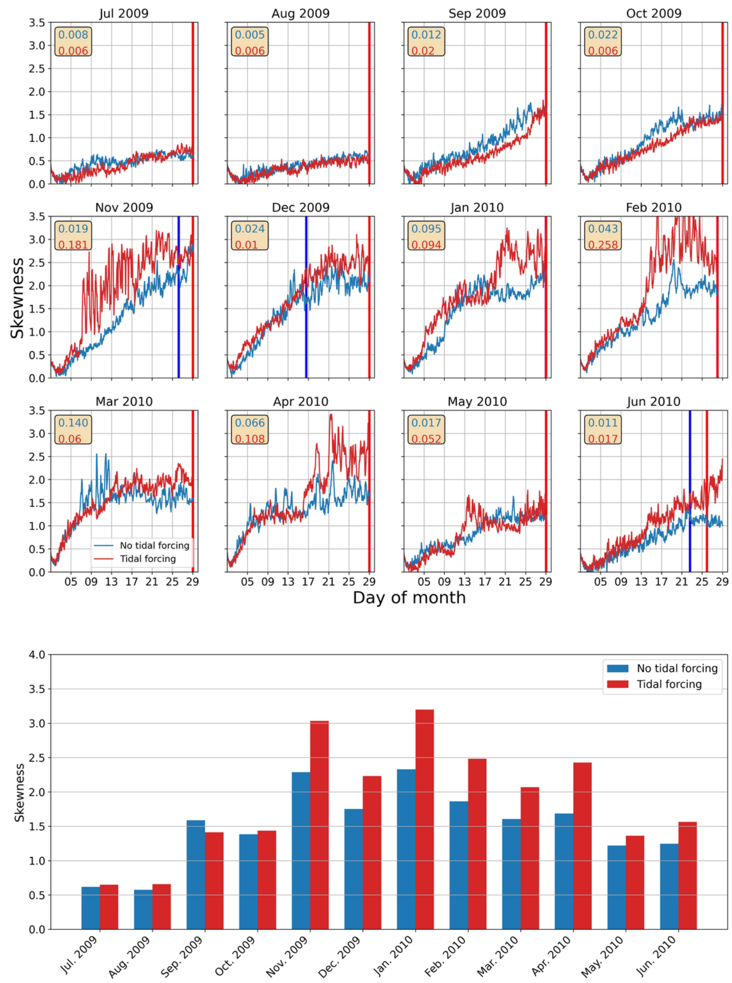

Figure 6: Skewness temporal evolution in time for each month for non-tidal (blue) and tidal (red) simulations. Values in the text box are the variance of the skewness from the beginning of the month till the vertical line. The vertical line indicates the moment in time when the first particle enters the subregion (see subsection 2.3.2.2). Bottom plot shows the skewness value at the vertical line.

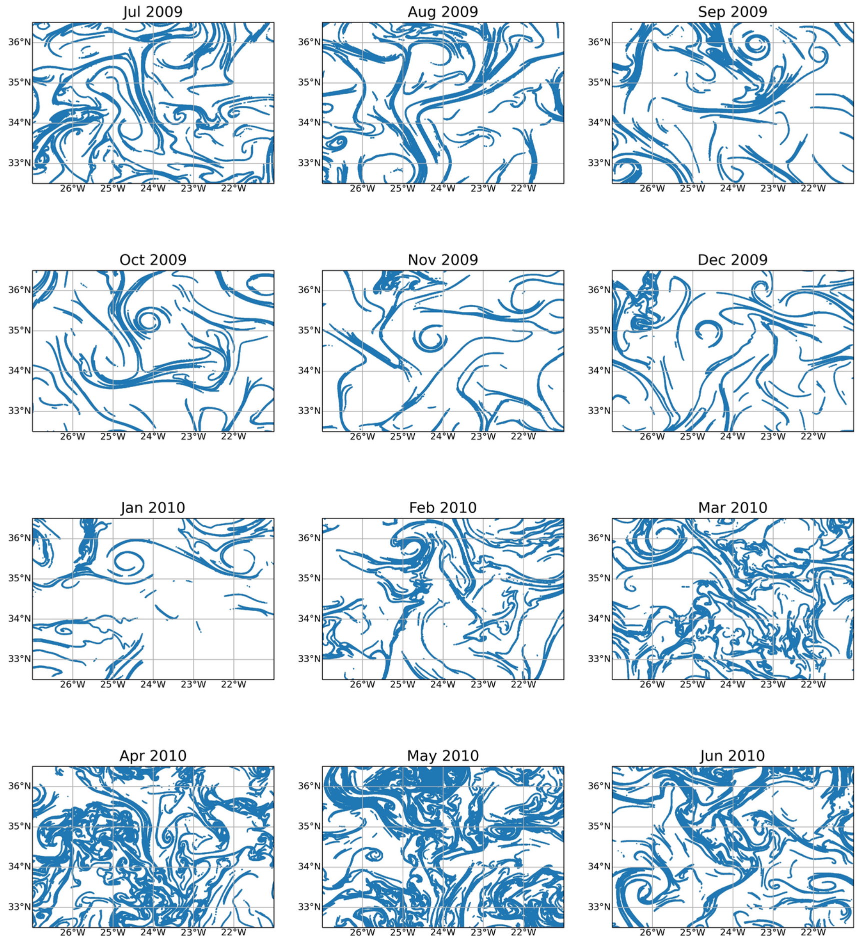

Figure 7: Attracting LCS structures on day 1 of each month for the non-tidal simulation.

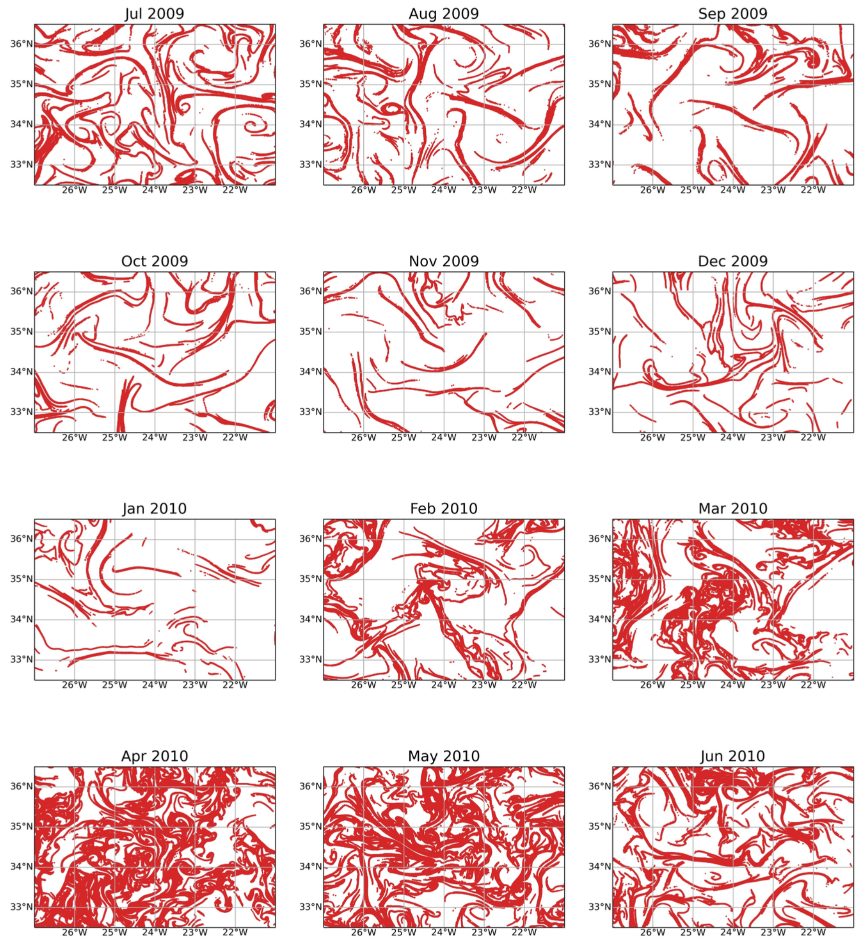

Figure 8: Attracting LCS structures on day 1 of each month for the tidal simulation.

Figure 9: Top: Percentage of virtual particles with backward FTLE > 0.5 days-1 . Bottom: Skewness values of the backward FTLE fields.

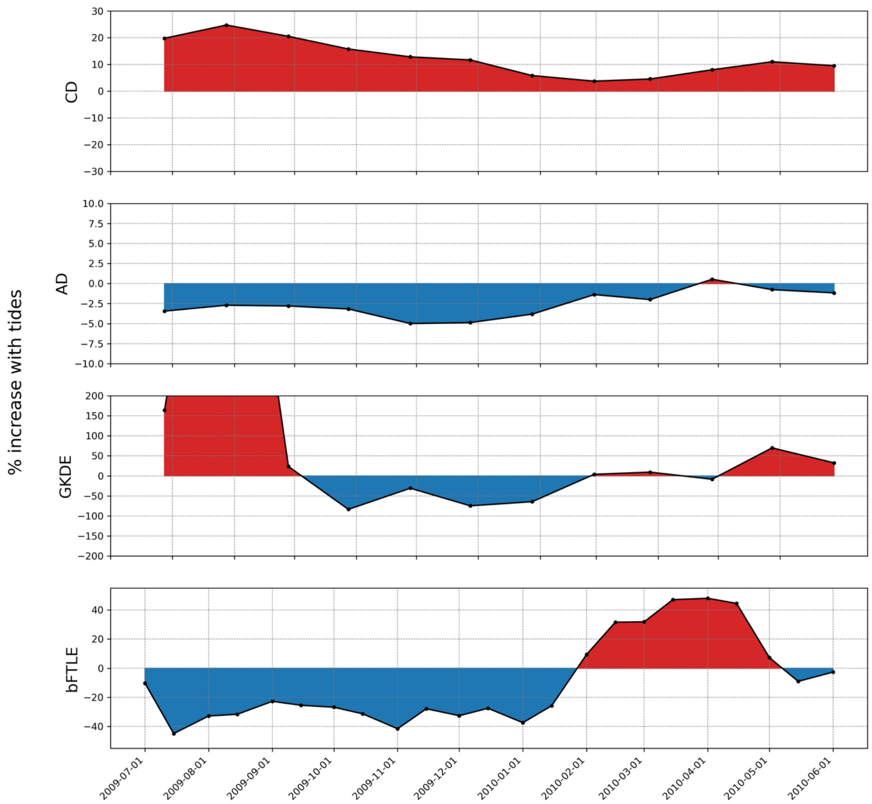

Figure 10: Percentage difference with tidal forcing per month for each diagnostic calculated. From top to bottom: cumulative distance (CD), absolute distance (AD), percentage of particles with high Gaussian Kernel Density Estimation (GKDE [?] 0.008) and percentage of particles with high backward Finite Time Lyapunov Exponents (bFTLE [?] 0.5 days-1).

Effects of tide induced dynamics on surface transport properties

Laura Gómez-Navarro[1], Erik van Sebille[1], Verónica Morales-Marquez[2], Ismael Hernandez-Carrasco[3], Aurelie Albert[4], Clement Ubelmann[5], Julien Le Sommer[4], Jean-Marc Molines[4], Laurent Brodeau[4]

[1]Department of Physics, IMAU, Utrecht University, Utrecht (The Netherlands)
[2]Université de Toulon, Aix Marseille Univ., CNRS, IRD, MIO, Toulon (France)
[3]Mediterranean Institute of Advanced Studies (IMEDEA, UIB-CSIC), Esporles, (Spain)
[4]IGE, UGA-CNRS-IRD-INP, Grenoble (France)
[5]Datlas, Grenoble (France)

Key Points:

- The analysis of the Lagrangian properties of a twin ocean model with and without tidal forcing shows different surface particle transport patterns.
- Absolute distances are smaller with tidal forcing while cumulative distances are larger.
- A greater temporal variability in surface particle accumulation patterns is present with tidal forcing.

Corresponding author: Laura Gómez-Navarro, `l.gomeznavarro@uu.nl`

Abstract

Understanding the pathways of floating material at the surface ocean is important to improve our knowledge on surface circulation and for its ecological and environmental impacts. Virtual particle simulations are a common method to simulate the dispersion of floating material. To advect the particles, velocities from ocean models are often used. Yet, the contribution of different ocean dynamics (at different temporal and spatial scales) to the net Lagrangian transport remains unclear. Here we focus on tidal forcing, only included in recent models, and so our research question is: What is the effect of tidal forcing on virtual particle dispersion at the ocean surface? By comparing a twin simulation with and without tidal forcing, we conclude that tides play an important role in horizontal Lagrangian dynamics. We focus on the Açores Islands region, and we find that surface particles travel a longer cumulative distance and a lower total distance with than without tidal forcing and a higher variability in surface particle accumulation patterns is present with tidal forcing. The differences found in the surface particle accumulation patterns can be more than a 40% increase/decrease. This has important implications for virtual particle simulations, showing that more than tidal currents need to be considered. A deeper understanding of the dynamics behind these tidal forcing impacts is necessary, but our outcomes can already help improve Lagrangian simulations. This is particularly relevant for simulations done to understand the connectivity of marine species and for marine pollution applications.

Plain Language Summary

At the surface of the ocean we can find a range of floating material e.g. algae, larvae, plastics and oil spills. Correctly simulating their trajectories is important to understand the ocean surface dynamics and their ecological, environmental and economical impacts. To simulate these trajectories, ocean currents data from ocean models are usually used. These ocean models try to represent different oceanic processes, and recent ones include the effect of tides. In this study we investigate how tides affect surface trajectories in a region south of the Açores Islands. We study the distances travelled by particles and how much they accumulate. We find that these are affected by tidal forcing and that the impacts on the accumulation patterns found are stronger or weaker depending on the size of the ocean structures analyzed. Therefore, we find that tides are im-

portant when studying oceanic surface trajectories. This has important applications for marine diversity studies and marine pollution forecasts.

1 Introduction

Understanding the pathways of floating material (e.g. larvae, plastics, oil and drifters) at the surface ocean is important not only due to its ecological and environmental repercussions (Sala et al., 2016), but also to improve our knowledge on the ocean dynamics (van Sebille et al., 2020; Chamecki et al., 2019). These floating material pathways can be studied by analysing horizontal particle dispersion properties. Understanding these 2D surface dynamics also helps to get some insights on the 3D dynamics, through the identification of strong convergence and divergence regions, that is, zones with significant vertical dynamics (e.g., d'Asaro et al., 2018; Hernández-Carrasco et al., 2018; McWilliams et al., 2019; Tarry et al., 2021). Identifying these zones has important implications for biology as they affect the supply of nutrients to the euphotic layer and therefore phytoplankton development (e.g., Lévy et al., 2001, 2012; Mahadevan, 2016). Understanding surface dispersion is not only useful to expand our knowledge on ocean dynamics, but also for practical issues such as better understanding the distribution of marine plastic (e.g., Onink et al., 2019), oil spills (e.g., Ainsworth et al., 2021), algae such as *Sargassum* (e.g., Miron et al., 2020; van Sebille et al., 2021) and larvae (e.g., Largier, 2003; Hidalgo et al., 2019; Díaz-Barroso et al., 2022). Identifying hotspots where pollutants or fish larvae accumulate can support ocean clean-up strategies and marine protected areas management, respectively (e.g., Poje et al., 2014; Krüger et al., 2017).

Simulating accurate trajectories of floating material in the ocean is complex as many processes at different spatiotemporal scales are involved (van Sebille et al., 2020). In this regard, the growing development of different sources of ocean velocity data has helped to analyse the impact of different dynamical scales on the transport processes: Ocean General Circulation Models (OGCMs) (e.g., Brunner et al., 2015; Sala et al., 2016), drifters (e.g., Maximenko et al., 2012; van Sebille et al., 2012), High-Frequency (HF) radar (e.g., Hernández-Carrasco et al., 2018; Révelard et al., 2021), altimetric satellite data (e.g., Beron-Vera et al., 2010; Liu et al., 2014) and other products like GlobCurrent (e.g., Onink et al., 2019) or a combination of them (e.g., Morales-Márquez et al., 2023). Nevertheless, limitations exist for these datasets because of their low spatial and/or temporal coverage or because of their low spatial resolution, for example, altimetric data. Current altimetric products do not capture all surface transport mechanisms (Bôas et al., 2019), especially those that are due to high-frequency motions such as internal tides and waves. OGCMs are not as limited by coverage and resolution, but to date they cannot resolve and represent all the different processes, like Langmuir circulation, and would need to be coupled to other models, like wave and biogeochemical models, to represent processes such as Stokes drift and bio-fouling, respectively (van Sebille et al., 2020; Tsiaras et al., 2021). Focusing on the open ocean, some of the processes that have received a great attention to improve the understanding of the surface transport properties from observations and numerical simulations, have been Ekman transport, Stokes drift and windage (e.g., Wenegrat & McPhaden, 2016; Iwasaki et al., 2017; Putman et al., 2020; Morales-Márquez et al., 2021; Morales-Márquez et al., 2023); especially in the context of marine debris (e.g., Maximenko et al., 2018; Dobler et al., 2019; Onink et al., 2019; Higgins et al., 2020). However, little attention has been paid so far to the effect of tides, and even less to the effect of internal tides (for example on the eddy field) and its impact on Lagrangian dynamics.

In this regard, a few studies have analysed the contribution of tidal induced dynamics to the transport of floating material, and only focused on tidal currents. Sterl et al. (2020) found that the impact of barotropic tidal currents on microplastic surface transport and accumulation was very small. Tidal currents have also been considered using the SMOC dataset (Drillet et al., 2019) to understand the trajectories of *Sargassum* in the Tropical Atlantic by van Sebille et al. (2021). Moreover, the Lagrangian transport due to internal tides has been studied by Sutherland and Yassin (2022), but they found it to be negligible when averaged over an inertial period. Technological advances in the past years have allowed recent OGCMs to include tidal forcing, improving the representation of internal wave fields (Le Sommer et al., 2018). Tidally forced OGCMs allow not only to consider tidal currents, but also the impact tides have on the flow structures, like eddies, filaments, or fronts. To our knowledge, no study looking at the impact of using velocity data from a tidally forced OGCM to simulate surface ocean trajectories has been done before.

Including tidal forcing in OGCMs can impact the flow field in different ways. It increases the energy at the fine-scales (here defined between 10 km and 100 km) as reported in Verron et al. (2020), where a higher Sea Surface Height (SSH) energy level is observed with than without tidal forcing at wavelengths below approximately 100 km.

This difference is more pronounced in the northern hemisphere summer (from hereafter seasons referring to northern hemisphere), when the high stratification conditions promote the generation and propagation of internal tides (Verron et al., 2020). One of the physical features that are responsible for this increase at the fine-scales are internal waves, which are ignored when only considering tidal currents and/or barotropic tides. Although internal waves occur at the interface between ocean layers (Arbic et al., 2018), their signal can sometimes be observed at the ocean surface (e.g., Jackson et al., 2012). Not only can they transport floating material (Shanks, 2021), but they can also affect the background flow, namely eddies, by altering their kinetic energy (Mtfller, 1976; Bühler & McIntyre, 2005; Barkan et al., 2017), as internal waves can lead to the extraction of mesoscale energy through dissipation (Barkan et al., 2017). Since mesoscale eddies can retain floating material for several days (e.g., d'Ovidio et al., 2013; Condie & Condie, 2016; Limer et al., 2020; Bello-Fuentes et al., 2021), this loss of energy could imply a loss of the coherence of their structure and thus of their capacity to accumulate/trap material. One of the main mechanisms that generate coherent eddy structures, are baroclinic instabilities (Stammer, 1997), and these can be modified by tidal forcing (Lin et al., 2023). While no specific research has been done on the impact of internal waves on the retention capacity of eddies, some studies have been done with surface waves. Dobler et al. (2019); Morales-Márquez et al. (2023) found that surface waves created by forcings like the wind and waves can have a significant effect on mesoscale structures like eddies, modifying their shape, and eventually reducing their retention capacity.

Our study region is located south of the Açores Islands, one of the areas in the North Atlantic with the highest internal waves signal (Ray & Zaron, 2016; Savage et al., 2017). These internal waves are generated by the interaction of the flow (tidal or current) with the bathymetry, especially during summer (June to September), when stratification is high (Jackson, 2004; Rocha et al., 2016; Torres et al., 2018; Lahaye et al., 2019; Verron et al., 2020). Moreover, this area has been found to be important in terms of marine pollution with a high exposure to marine floating debris, which reaches the islands through filaments and eddies generated from the Gulf Stream (Sala et al., 2016; Pham et al., 2020; Cardoso & Caldeira, 2021).

Our objective is to investigate the effects of tide induced dynamics on surface transport properties. In Section 2 we describe the dataset used and the methods to evaluate the data. Section 3 describes the results obtained and in Section 4, we discuss them and suggest future studies.

2 Data and methods

2.1 The extended North Atlantic simulation at 1/60 ° (eNATL60)

eNATL60 is an extended version of the NATL60 run (see Ajayi et al. (2020); `https://github.com/meom-configurations/NATL60-CJM165`) in which a larger spatial domain is covered. The model's domain includes the North Atlantic basin: from 6°N to 66°N and from 80°W to 9.5°E (fig. 1), together with the whole Mediterranean and Black Seas and the Gulf of Mexico (not shown).

With a spatial resolution of 1/60 ° and a model time-step of 40 seconds, the simulation is submesocale permitting (Verron et al., 2020). For the scope of this study, we use the hourly model outputs, and though the model is 3D, we only use the 2D surface velocity fields. Two simulations have been produced with this configuration: a twin experiment without and with tidal forcing (Brodeau et al., 2020a, 2020b). The tidal constituents used are M2, S2, N2, K1, O1 (Brodeau et al., 2020b), and the presence of tidal forcing allows the conversion of tidal energy into the internal wave field. This conversion happens through the interaction of wave and unbalanced motions, and via flow-topography interactions (Arbic et al., 2018). The simulation timespan is from mid-June 2009 to October 2010 (simulation years, no data assimilation included). Verron et al. (2020) compared the simulation outputs to the altimeter SARAL/Altika, focusing on a spectral comparison with the simulation's surface data. They found that at the large scales (down to approximately 80 km) the model's SSH spatial spectra is very close to that of SARAL/Altika, for both the non-tidal and tidal run. The high frequency motions eNATL60 have been compared to altimetry by Ansong et al. (2020), showing a slight overestimation of SSH variance in the tidally forced run due to no explicit wave drag in the simulation. This set of simulations present an unprecedented opportunity due to its high spatial and temporal resolution, and its twin simulation characteristic with and without tidal forcing.

2.2 Particle trajectory simulations

The OceanParcels Lagrangian framework v2.2.2 (Delandmeter & van Sebille, 2019) is used to simulate 2D trajectories of virtual particles at the sea surface. A fourth or-

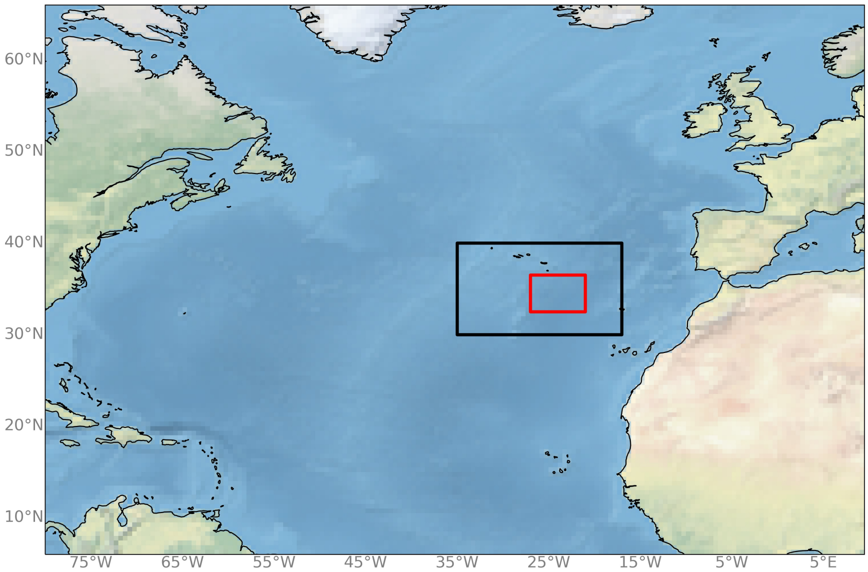

Figure 1. Spatial domain of the eNATL60 simulation (except the Gulf of Mexico, Black Sea and eastern Mediterranean Sea domains). Black box shows the region of this study where virtual surface particles are released. Red box shows the subregion used for some of the analyses.

der Runge-Kutta particle advection scheme is used with a run-time time-step (dt) of 5 minutes. We consider infinitesimal passive and buoyant particles. Two types of simulations are done. Firstly, particles are released monthly at the surface over the whole region (black box in fig. 1) with a 0.04° spacing, making it a total of 106926 particles. Particles are advected for 28 days, from July 2009 to June 2010. Particles are advected using the velocity field obtained from the outputs of the two model simulations without and with tidal forcing (eNATL60). Particles which leave the domain (black box in fig. 1) are removed. Secondly, to calculate backward Finite Time Lyapunov Exponents (bFTLEs), particles are released every 0.004° and advected for 14 days (biweekly) for the same period as the previous diagnostics (July 2009 to June 2010). Due to the computational cost, bFTLEs are calculated at the subregion shown in fig. 1 (red box). Further details on the bFTLEs computations and parameterizations are given in Section 2.3.2.3.

2.3 Lagrangian diagnostics

To evaluate the impact of tidal forcing on the surface particle trajectories, we use a range of Lagrangian diagnostics that allows us to obtain information about the transport properties at different temporal and spatial scales. We evaluate the effect of tidal forcing on particle dispersion by analyzing two Lagrangian properties: the distance travelled by the particles and their surface accumulation.

2.3.1 Distance travelled

We evaluate the absolute distance (AD) and the cumulative distance (CD) travelled by each particle. AD is the shortest distance between the initial and final point of a particle's trajectory. It tells us about the absolute (or net) distance travelled by the particle in a period, T, with respect to their initial position. CD is the sum of all the distances travelled during each time-step, and it gives us an idea about the total distance explored by the particle. They are defined as:

$$AD(x, y, t = T) = r(t = T) - r(t = 0) \tag{1}$$

$$CD(x, y, t = T) = \sum_{n=1}^{T} (r(t) - r(t-1)) \tag{2}$$

; where r(t) = f(x,y) and is the position of the particle at time, t.

2.3.2 Surface accumulation patterns

The analysis of the surface particle accumulation is more complex and requires different statistical and diagnostic techniques. These diagnostics are sensitive to the parameters, presenting a higher associated uncertainty than the other metrics based on the travelled distances. We also analyse the impact of the tidal forcing on the transport barriers computing pair of particles metrics like the Finite Time Lyapunov Exponents. Consequently, we use a range of different techniques which are described below.

2.3.2.1 Gaussian Kernel Density Estimation (GKDE) One of the methods used to calculate the density of particles is a 2-dimensional horizontal Gaussian Kernel Density Estimation (GKDE). This is a non-parametric (applicable to a non-Gaussian distribution) estimate of the probability density function of a field. The GKDE is applied monthly on all particles in the whole domain (black box in fig. 1) by calculating it on the particle distribution of day 28. We use the python SciPy stats gaussian_kde algorithm with a default kernel size (bandwidth), which is calculated following Scott's Rule (Scott, 1992). This bandwidth selector calculates the optimal bandwidth value that avoids both over-smoothing and under-smoothing.

2.3.2.2 Particle density histogram skewness The particle density is also investigated using histograms. A two-dimensional histogram of the particles' monthly positions in the final step is calculated with a bin size of 0.1° by 0.1°. It is calculated for the subregion shown by a red box in fig. 1. This subregion is selected as to avoid regions without particles, which appear as white intrusions and are present in all months (for example the white region at the west in the no tides September GKDE subplot of fig. 3). The GKDE is calculated on each particle, so the effect of the region borders is smaller than on the 2D histogram. Then, a one-dimensional histogram (10 bins) of the number of particles in each bin is calculated from it to show the frequency of the 2D bin counts.

The skewness of the 2D histogram fields is analysed. This can give us information on the occurrence of extreme events (e.g., White, 1980), and therefore the occurrence of high accumulation zones (i.e., high 2D bin count).

2.3.2.3 Backward Finite Time Lyapunov Exponents (bFTLEs) Finite Time Lyapunov Exponents (FTLEs) is a Lagrangian diagnostic for describing relative dispersion properties of fluid flows, providing information on the position of oceanic transport barriers, the so-called Lagrangian Coherent Structures (LCS) (Boffetta et al., 2001; Haller, 2015). FTLEs is based on Lagrangian separation rate of two infinitesimally close trajectories, which grows exponentially over time (Haller, 2001; Shadden et al., 2005). It measures the separation rate of a pair of particles after a fixed time interval (Shadden et al., 2005) (equivalent to Finite Size Lyapunov Exponents (Hernández-Carrasco et al., 2011), which measure the separation rate of two particles, but fixing the final separation distance). Ridges of backward FTLE (bFTLE) fields reveal lines of maximum stretching, identifying attracting LCS. Since particles cannot cross them, the LCS determine the flow motion, providing the main transport pathways (Haller & Yuan, 2000; Shadden et al., 2005). Recent studies have shown the relationship between attractive LCS with filaments of accumulated negative Lagrangian horizontal divergence of velocity fields, revealing regions of particle aggregation (Huntley et al., 2015; Hernández-Carrasco et al., 2018).

Based on Shadden et al. (2005), FTLE can be derived considering the stretching of two neighbouring particles, initially separated a distance δ(t0), and advected in the flow after a fixed time of integration (τ), when both particles will be separated $\delta(t_0+\tau)$. We obtain the following expression for the FTLE in two-dimensional flows, denoted as $\lambda(x, y, t)$, which depends on the position and time,

$$\lambda(x, y, t) = \frac{1}{\tau} * ln \frac{\delta(t_0 + \tau)}{\delta(t_0)} \tag{3}$$

Following Shadden et al. (2005), to obtain the FTLEs we compute the maximum eigenvalues of the Cauchy-Green deformation tensor after the integration time (τ) defined in Haller (2001).

The initial particle separation, $\delta(t_0)$, is set to be of 0.004°, which is finer than the eNATL60 velocity field grid (0.0167°) and $\tau = 14$ days. This allows a better identification of the subgrid structures originated by chaotic advection (see Hernández-Carrasco et al. (2011, 2020)). Finally, bFTLEs are calculated biweekly, on day 1 and 15 of each month. A two-weeks integration time was chosen because with $\tau = 28$ days we obtained bFTLE results with a high uncertainty, and for one week of integration time we found that the coherent structures are not fully identified.

3 Results and discussion

Firstly, we look at the impact of tidal forcing on the distance travelled by the particles. We compare the cumulative distance travelled (CD, sum of all the distances travelled during each time-step) and the absolute distance travelled (AD, the shortest distance between the initial and final point of the particle's trajectory). Fig. 2 shows that the particles travel a large range of distances after 28 days, but if we focus on the median values shown in the box plot, we observe differences between the travel distances with and without tidal forcing. The median CD values are higher for the tidal than for the non-tidal simulation, up to a 25% larger in August with respect to the non-tidal simulation. This could be explained by the elevated presence of high-frequency motions in the tidal simulation (Verron et al., 2020), inducing small and highly fluctuating perturbations in the particle motions, which results in a longer CD or total particle trajectory. For the median AD values (fig. 2 (bottom)), the opposite is observed: larger ADs are travelled by the particles in the non-tidal than in the tidal simulation. For some months, the non-tidal simulation values of the median are only slightly higher than the tidal values, but the percentile 75 values of most months also reflect this pattern. This suggests that tidal forcing induces small scale oscillations that increase particle trajectory length (CD), but slightly decreases the absolute distance travelled (AD). This implies that particle trajectories explore more of the ocean surface because of tidal forcing.

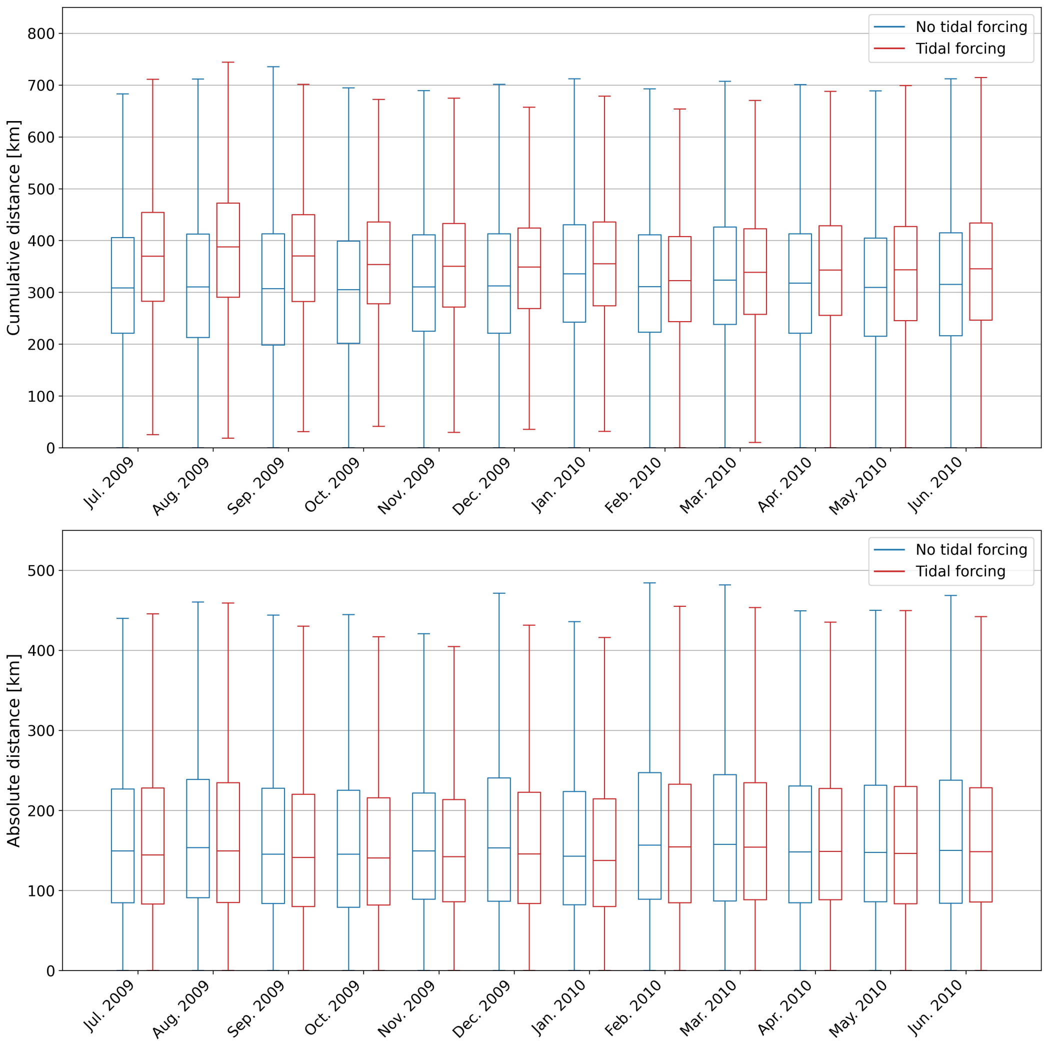

Figure 2. Box plots of mean cumulative distance [km] (top) and mean absolute distance [km] (bottom) travelled by the virtual particles per month.

Next, we analyse the impact of the tidal induced dynamics on the surface particle accumulation using the GKDE. The results obtained here using the optimal kernel size (see Section 2.3.2.1), seem to reflect the surface particle accumulation at mesoscale spatial scales. This can be observed in the red and yellow eddy mesoscale-like structures observed in fig. 3. A higher presence of very high-density regions (red colour) can be observed in winter than in summer, for both simulations (with and without tidal forcing). This implies a higher surface particle accumulation in winter (December to March) than in summer (July to September 2009 and May and June 2010). This could be due to the higher number of eddies present in winter than in summer (Ajayi et al., 2020) and their associated capacity to accumulate floating material (e.g., d'Ovidio et al., 2013; Condie & Condie, 2016; Limer et al., 2020; Bello-Fuentes et al., 2021). We observe that this summer-winter difference is lower in the tidally than in the non-tidally forced simulation. When tides are included, the surface particle accumulation increases in summer and reduces in winter. Fig. 4 shows the percentage of particles with a high GKDE value (GKDE > 0.008) per month, identified as the yellow and red regions in fig. 3. This corresponds to a GKDE threshold of 0.008, which is value that reflects high particle density for all months in both simulations.

The seasonal variability of GKDE can be related to changes in the eddy and internal waves fields. The increase of GKDE in the summer months could be explained by a higher presence of internal waves in the tidally forced simulation. The higher presence of internal waves in summer occurs because it is when stratification is the highest. These internal waves can create more convergence zones (Shanks, 2021). The lower accumulation capacity during winter could be associated with a decrease of the energy at the mesoscale lead by the dissipation effect of internal waves (Barkan et al., 2017). This could reduce the capacity of mesoscale eddies to accumulate surface material, as similarly found to happen with surface waves (Dobler et al., 2019; Morales-Márquez et al., 2023). On the other hand, the presence of internal waves in winter is lower than in summer (Jackson, 2004; Rocha et al., 2016; Torres et al., 2018; Lahaye et al., 2019; Verron et al., 2020). Therefore, the lower particle accumulation in winter with tidal forcing, could also be explained by the fact that the flow convergence associated with mesoscale dynamics is attenuated by the effect of more energetic small-scale dynamics induced by tides. This is observed by Verron et al. (2020), which show how the energy levels (power spectral densities) of eNATL60 at the fine-scales increases with tidal forcing. Moreover, Haza et al. (2016) found that the presence of submesoscale structures makes the mesoscale eddy structures more permeable, explaining this lower accumulation with tidal forcing in winter. Overall, the GKDE diagnostic (figs. 3 and 4) shows that including tidal forcing significantly impacts surface particle accumulation patterns.

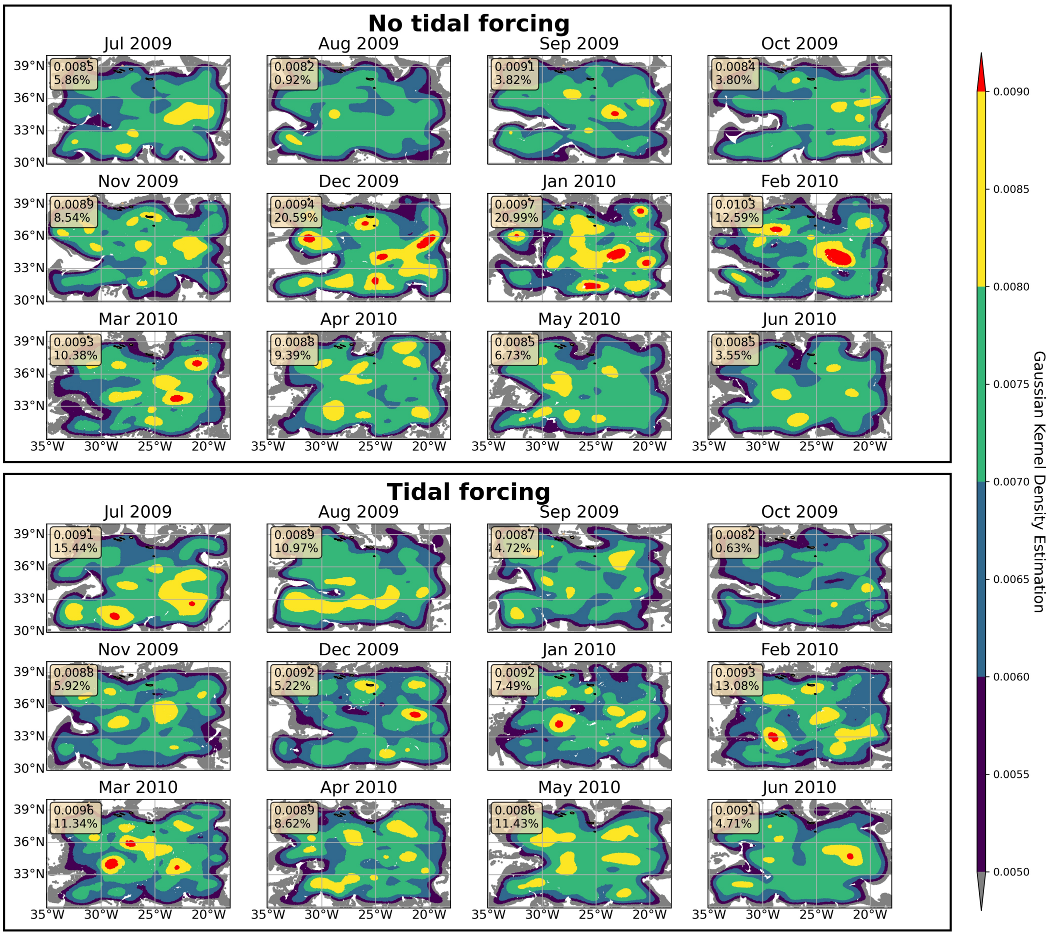

Figure 3. Gaussian Kernel Density Estimation (GKDE) comparison between non-tidal (top) and tidal (bottom) simulations. Maximum GKDE value (top) and percentage of particles with a high GKDE value (greater than 0.008) (bottom) are shown in the bottom left textbox.

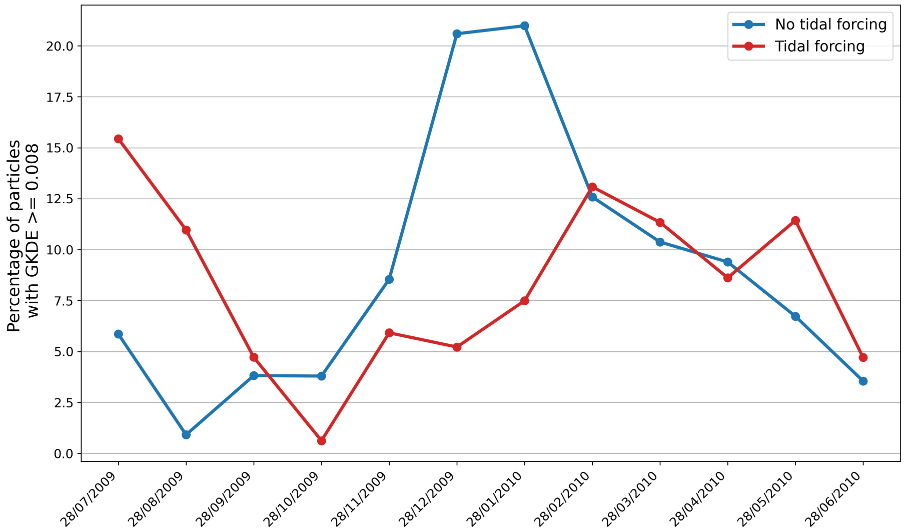

Figure 4. Comparison of the percentage of particles with a high GKDE value (greater than 0.008) per month. Non-tidal results are shown in blue and tidal in red.

To study the surface particle accumulation from another perspective, 2D histograms of the particles' distribution in the final time-step are also analysed. Figure 5 shows the monthly 1D histograms of the 2D histogram bin counts. It shows that all the probability density functions (1D histograms) of the surface particle accumulation (2D histograms) are positively skewed. Qualitatively, no big differences are observed between the non-tidal and tidal histograms. The vertical, dashed line in fig. 5 shows the maximum value of the 2D histograms bin counts. The particle density maximum is greater for the tidal than the non-tidal in 7 out of 12 months (August, December, January, February, March, April, and June). No clear pattern is observed in the maximum, though greater values are reached in the tidal simulation. This means that zones with much higher accumulation can occur when tidal forcing is included.

Deeper analysis of the positive skewness of the histograms gives us insight on extreme events, which is linked to high surface particle accumulation. Figure 6 (top) shows the temporal evolution of the skewness of the one-dimensional histogram (fig. 5) of the particle density (from the two-dimensional histogram). Both the non-tidal's and tidal's skewness increase with time. The final skewness value is calculated at the time when the first particle released at the boundary of the region (black box fig. 1) enters the subregion (red box fig. 1), and it is represented by the vertical line in fig. 6. This is done to

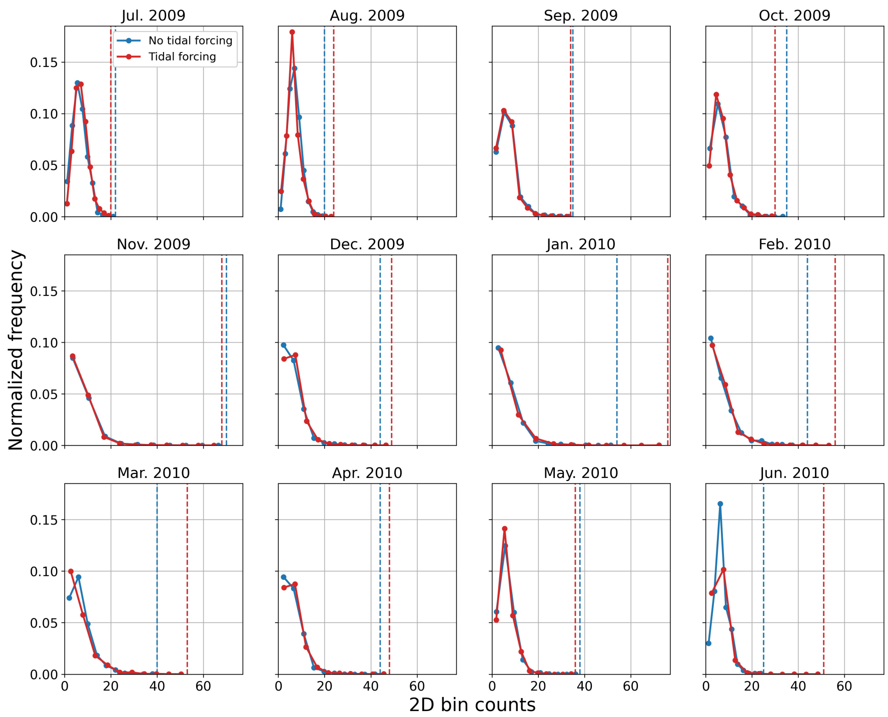

Figure 5. 1D histogram of the 2D histogram of the distribution of the particles after 28 days of advection. Results of the non-tidal simulation are shown in blue and from the tidal in red. Vertical, dashed lines indicate the maximum value.

minimize and homogenize the impact of the simulation boundary effects. The final skewness values for each month are shown in fig. 6. Except for September, all months have higher skewness values in the tidal than the non-tidal simulation. For most months, the skewness' temporal variability is highest for the tidal simulation. The temporal variance of the skewness (until the vertical line) is shown in the text boxes in fig. 6 (top). For 6 out of the 12 months it is higher for the tidal simulation, in 3 of the months the values are very close (0.002 difference or less) and in the 3 other months it is higher for the non-tidal simulation.

The backward FTLEs give us information on the attracting LCS, identifying transport barriers, and filaments of coherent convergence. It gives us more details at finer scales than the GKDE and the 2D histograms as it can identify subgrid structures present (see

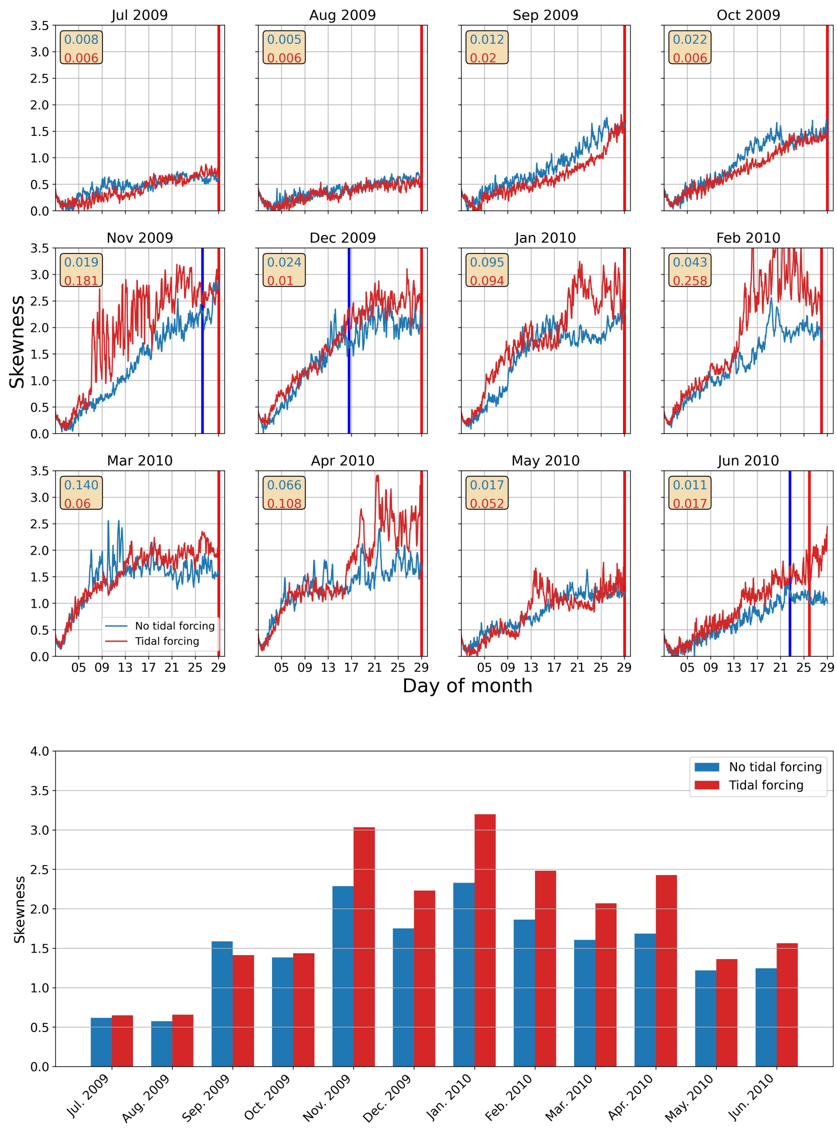

Figure 6. Skewness temporal evolution in time for each month for non-tidal (blue) and tidal (red) simulations. Values in the text box are the variance of the skewness from the beginning of the month till the vertical line. The vertical line indicates the moment in time when the first particle enters the subregion (see subsection 2.3.2.2). Bottom plot shows the skewness value at the vertical line.

section 2.3.2.3). Moreover, FTLEs describe the surface particle accumulation patterns by identifying the outline of the accumulation zones, whilst the GKDE and histogram diagnostics identify the area of the accumulation zone due to eddies or other LCS. We consider that for this region, the backward FTLE fields (see Figures S1 and S2 in the supporting information) reflect high flow convergence values above 0.5 $days^{-1}$. This threshold is selected based on the characteristics of the bFTLE probability density function (PDF). It generally represents for all months, the smallest bFTLE value of the asymmetric tail of the PDF (see fig. A1) associated with intermittent dynamics and identified here with maximum bFTLE values organized in filament-like structures.

Figures 7 and 8 show the attracting LCS on day 1 of each month for the non-tidal and tidal simulations, respectively. We can observe how eddy structures are much sharper in the non-tidal than tidal simulations, specially from September to January. This coincides with the GKDE results in winter, for both diagnostics the identified surface particle accumulation patterns decrease in winter. Qualitatively, from July to January we can observe less attracting LCS with tidal forcing (fig. 8) than without (fig. 7), and we quantify this and its distribution in fig. 9. The top panel shows the percentage of particles in the final time-step (after 14 days) with a bFTLE greater than 0.5 $days^{-1}$. For the summer, autumn and beginning of winter months (from July to December 2009 and, January and June 2010), non-tidal FTLEs exhibit higher values than the tidal values. The percentage of particles with high bFTLE values is decreased down to $\sim$40% of the non-tidal value, when tidal forcing is used. During the end of winter and spring, the opposite happens, and the percentage of particles increases up to $\sim$50% with tidal forcing. For both the non-tidal and tidal simulations, the highest percentage of particles with a bFTLE larger than 0.5 is obtained in April, and another smaller peak seems to be present in July. This observed seasonal variability in the bFTLE high values is larger for the tidal than for the non-tidal simulations.

Some differences between GKDE and bFTLE are observed in the months of maximum particle accumulation and in the seasonal variability. While the maximum peak in the GKDE is obtained in January for the non-tidal simulation, the maximum bFTLE is obtained in April and for the tidal simulation. Also, the maximum bFTLE for both simulations is in April, but the maximum GKDE is in different months: January for the non-tidal and July for the tidal simulation. Then, from autumn to winter (October 2009 to March 2010), both for the GKDE and the bFTLE the same relationship between the surface particle accumulation patterns in the non-tidal and tidal simulations is observed: from October to January the non-tidal is highest, and in February and March the tidal is highest. From July to September 2009 and April to June 2010, the relationship between the non-tidal and tidal is opposite in the GKDE and bFTLE fields. These months coincide with the maximum probability of internal waves observation in the Açores Islands (Jackson, 2004). Considering that internal waves promote the transfer of energy from the mesoscale to the submesoscale (Barkan et al., 2021), that their presence is more pronounced with tidal forcing, and that bFTLEs capture better the fine-scale and the GKDE the mesoscale transport dynamics; the tidal forcing affects the FTLE and GKDE diagnostics differently. We see then an increase in the bFTLE fields (fine-scales) and a decrease in the GKDE fields (mesoscale) with the tidal forcing simulation. Lastly, it is important to note that a subregion is used for the bFTLE calculation (due to calculation costs) while the GKDE is computed for the whole region. A sensitivity analysis (not shown) of GKDE to different areas was performed, obtaining no significant differences in the resulting accumulation patterns. Therefore, these different Lagrangian simulation characteristics are not responsible for the surface particle accumulation discrepancies observed between both Lagrangian metrics.

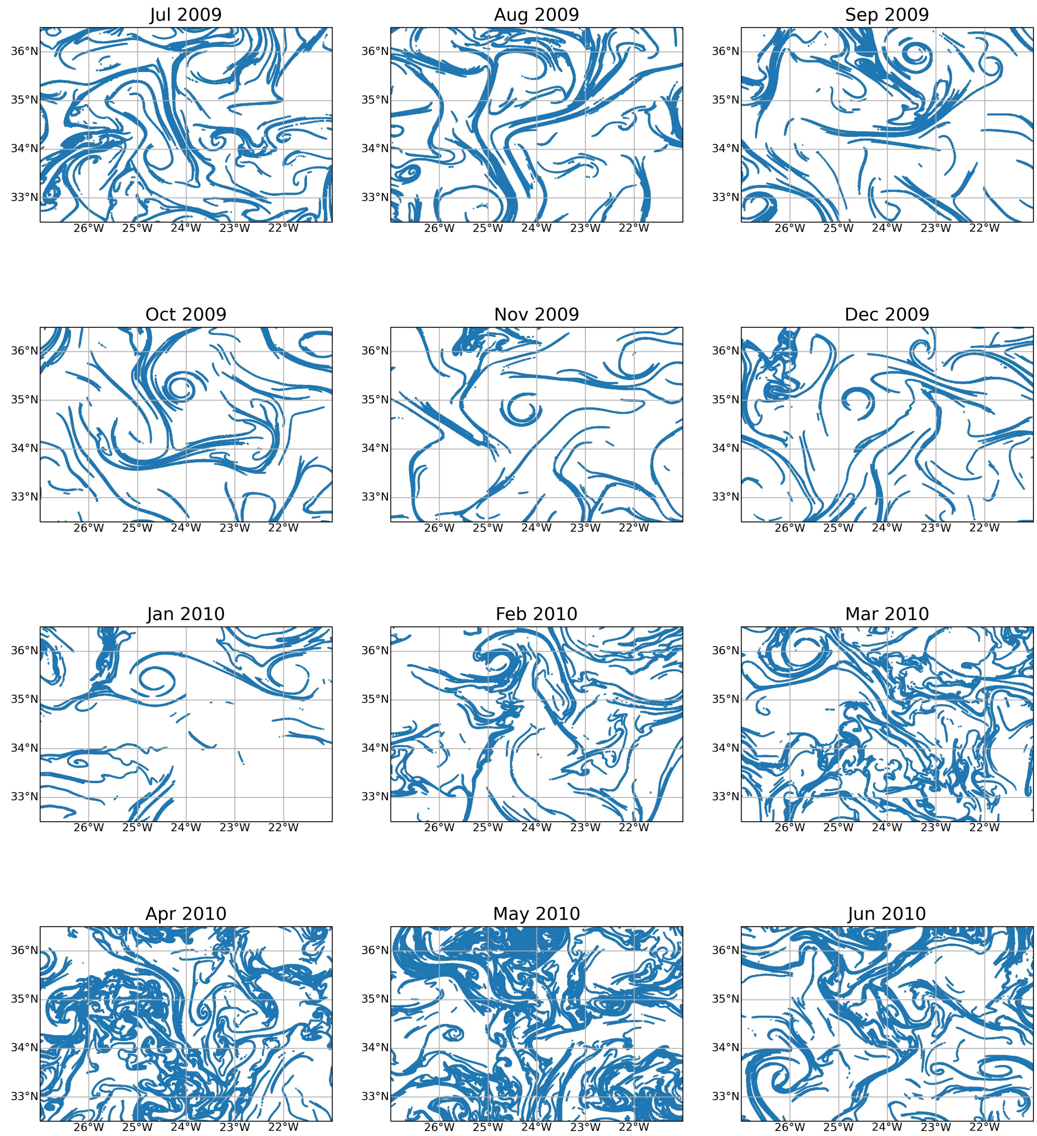

Figure 7. Attracting LCS structures on day 1 of each month for the non-tidal simulation.

Fig. 9 (bottom) shows the skewness value of the bFTLE fields. For most months, it is higher with than without tidal forcing, or they are very close (except from 15/03/2010 to 15/04/2010 (inclusive)). This is consistent with the higher skewness values of the 2D bin counts histograms obtained for most months when tidal forcing is included. This suggests that tides induce a higher occurrence of areas with extreme values of high particle accumulation, which could have an impact on the appropriate prediction of surface clustering areas.

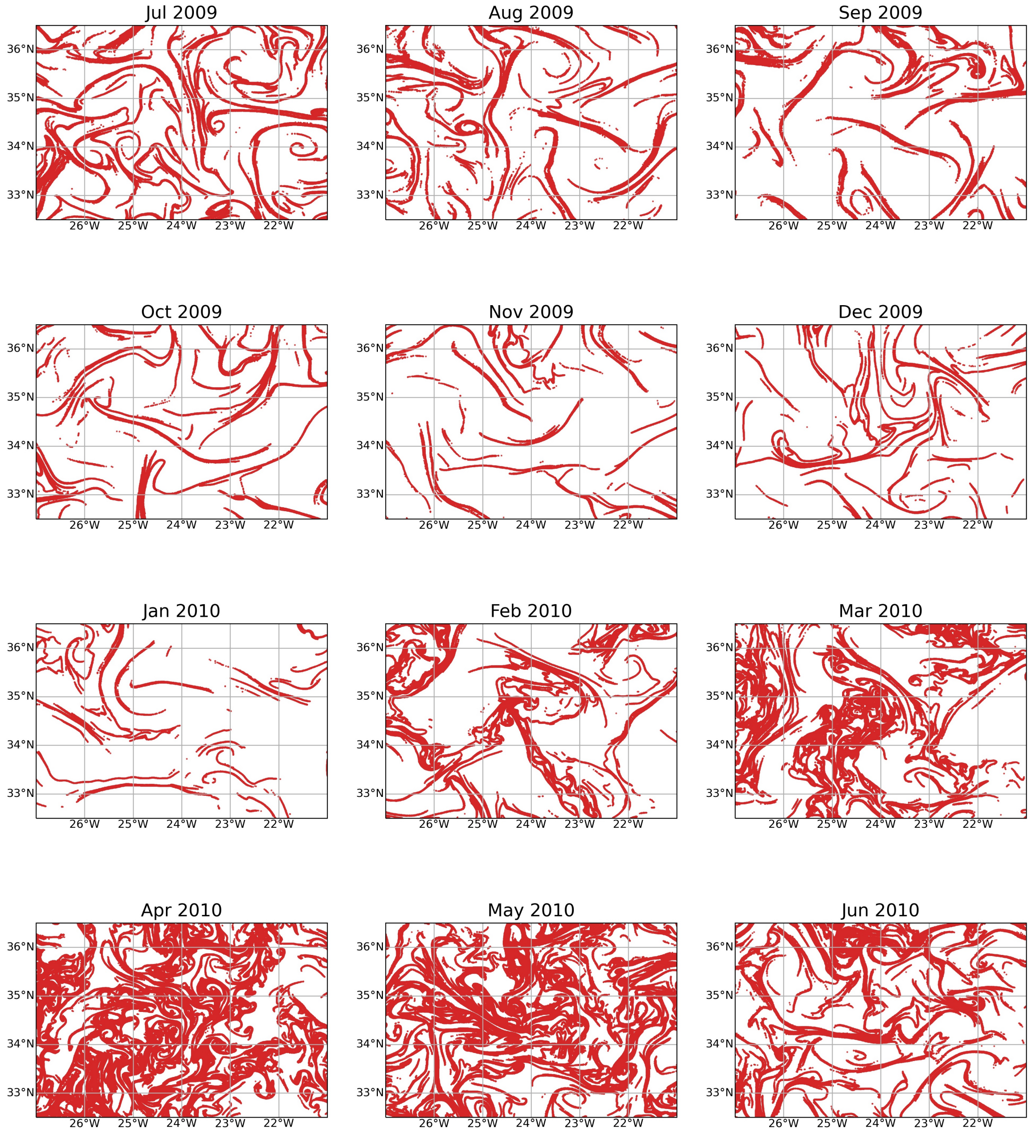

Figure 8. Attracting LCS structures on day 1 of each month for the tidal simulation.

Lastly, we quantify the impact of including tidal forcing in the above diagnostics. We do this by calculating the percentage increase or decrease of the tidal value with respect to the non-tidal value (eq. 4). As observed above, the impact varies depending on the diagnostic. CD shows a greater change than AD when tidal forcing is used (fig. 10. The increase in CD ranges from 3.75% to 24.77% and the decrease in AD from 0.76% to 4.99%. Even if these percentage values seem low, even the lowest of them (0.76% decrease in AD), translates to a difference of 112 km which is substantial in terms of clean-up strategies and the management of marine protected areas. For the GKDE, the high-

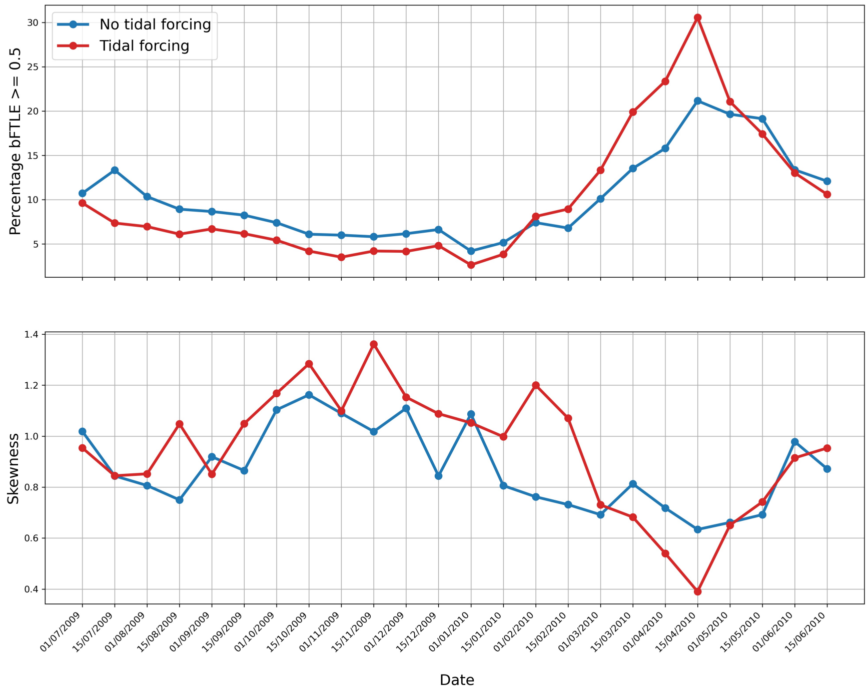

Figure 9. Top: Percentage of virtual particles with backward FTLE > 0.5 $days^{-1}$. Bottom: Skewness values of the backward FTLE fields.

est change is observed, reaching values above 40% in several months. The impact of tidal forcing is highest in August 2009 when it reaches a very high % (not shown in fig. 10) equivalent to the GKDE surface accumulation becoming 12 times higher. Although during most of the months the tidal forcing causes GKDE to increase, for 4 months (October to January) it decreases. In October-December 2009 and January 2010 the percentage of particles with a high GKDE value (high particle density) is reduced between 30% and 84% when tidal forcing is included, while in July-September 2009 and May-June 2010, it is increased between 23% and 1095% (fig. 4). For the rest of the months the increase/decrease is less than 10%.

For bFTLE, between February and May it increases, and decreases for the rest of the months, reaching % changes of around 40% (increases and decrease). During the end of autumn and winter months (October to February), there is a negative impact like with GKDE. This could mean that some dynamics affected by tidal forcing, like baroclinic instabilities, could be disturbing the eddy field which determines these two accumulation patterns. Previously it was mentioned that tidal forcing could affect the already existing eddy field, but we could also consider that it could affect the formation of eddies. Lin et al. (2023) found that with tidal forcing there is an increase in vertical mixing and thus a change of stratification that decreases baroclinic instabilities. Ajayi et al. (2020) showed that for the North Atlantic baroclinic mixed layer instabilities are responsible for an increase of submesoscale eddies in Winter. In general, this quantification of the impact of tidal forcing on the surface transport patterns, shows that although the impacts are different throughout the year and at different spatial scales, this forcing should be considered when wanting to carry out Lagrangian analyses where the surface transport patterns are important. Especially when these analyses are to be used, for example, for ocean pollution clean-up strategies (e.g. Poje et al., 2014).

$$\%\ difference = \frac{(X_T - X_N)}{X_N} * 100 \tag{4}$$

; where X is the value for each of the different diagnostics (CD, AD, percentage of GKDE ≥ 0.008 and percentage of bFTLE ≥ 0.5), for tidal (X_T) and non-tidal simulation (X_N).

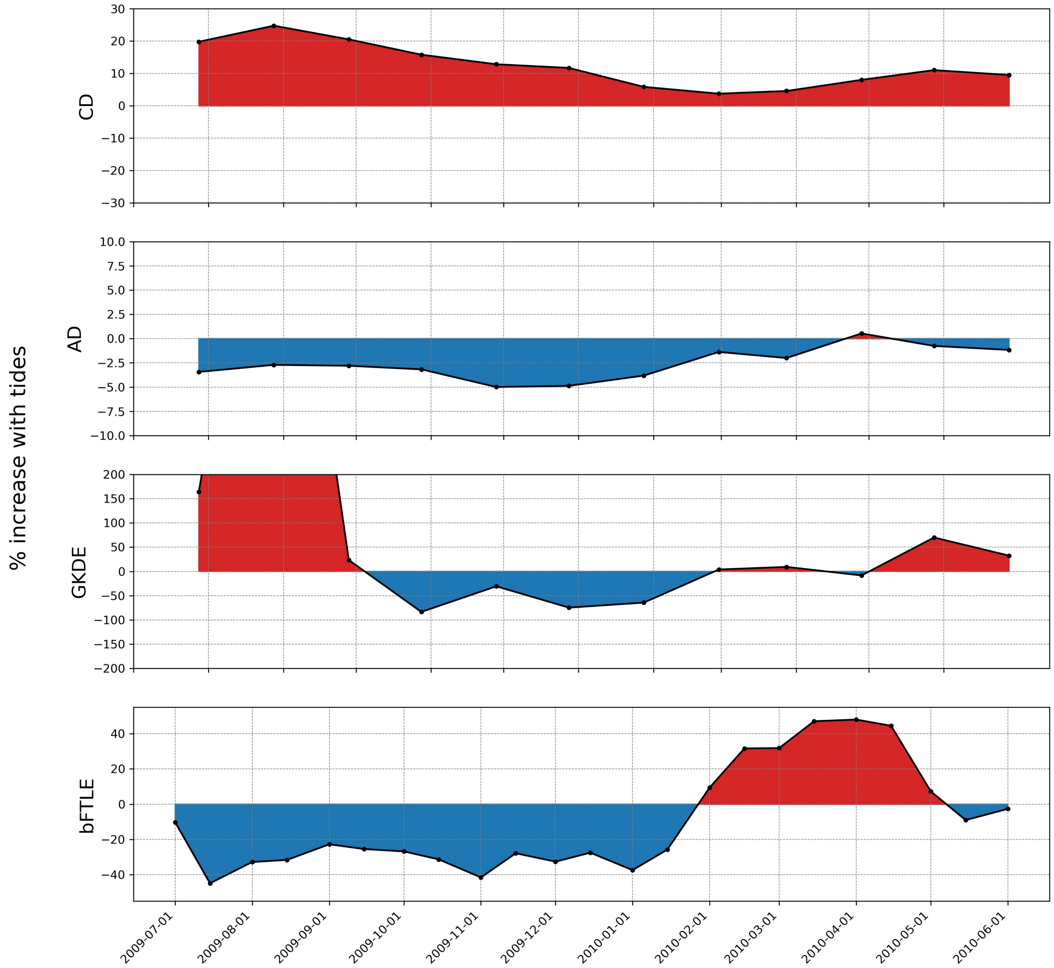

Figure 10. Percentage difference with tidal forcing per month for each diagnostic calculated. From top to bottom: cumulative distance (CD), absolute distance (AD), percentage of particles with high Gaussian Kernel Density Estimation (GKDE ≥ 0.008) and percentage of particles with high backward Finite Time Lyapunov Exponents (bFTLE ≥ 0.5 $days^{-1}$).

4 Conclusions and perspectives

This study aimed to investigate the impact of tide induced motions on Lagrangian dynamics, focusing on surface accumulation. A NEMO North Atlantic twin simulation with a resolution of 1/60° (eNATL60) without and with tidal forcing was used to advect surface virtual particle trajectories in a region around the Açores Islands. The results show that tides play an important role in the surface distribution of particle accumulation regions and dispersion properties. The impact of the tidal induced dynamics on

Lagrangian dispersion is quantified by computing the distances travelled by the virtual surface particles, and on the accumulation of particles detected at different scales.

Firstly, when we look at the monthly distances travelled by particles, longer cumulative distances are travelled in the tidal run, but shorter total distances than in the non-tidal run. This implies that particle trajectories explore more of the ocean surface because of tidal forcing, which can have important implications in terms of pollution impacts. To analyse the patterns of surface particle density we use three diagnostics: Gaussian Kernel Density Estimation (GKDE), 2D histograms and backward Finite Time Lyapunov Exponents (bFTLEs). The GKDE analyses seem to represent the mesoscale accumulation, and they show that with tidal forcing, the accumulation increases during the summer months and decreases in the winter months. The 1-dimensional histograms of the particle density (2-dimensional bin counts) show that all monthly distributions are positively skewed. We look at the temporal evolution of this skewness, and we find a high temporal variability, especially for the tidal forcing simulation. After one month, the skewness is higher for the tidal than the non-tidal forcing simulation for all months, except for September. Lastly, we calculate the bFTLEs which can be used as a proxy of convergence flow structures and capture smaller scale dynamics than the previous techniques. We find that in summer, the simulation without tides has a higher percentage of particles with higher bFTLE values than the tidal simulation. For the winter months, the opposite is obtained, except for January. We find that the skewness of the bFTLE fields is also higher for the tidal than the non-tidal simulation for most months. Therefore, adding tidal forcing can create a higher occurrence of extreme events, that in this case correspond to regions of high surface particle accumulation.

Several explanations could be behind these results. Barkan et al. (2021) found that when internal wave forcing was used in their simulations (which could be analogous to the tidal forcing used here, as it creates a higher presence of internal waves), less mesoscale kinetic energy is present both in summer and winter. The energy is transferred towards submesoscale fronts and filaments, particularly in winter (Barkan et al., 2021), and this could impact on the coherence of the mesoscale eddies, reducing their capacity to trap particles in a higher presence of submesoscale structures (Haza et al., 2016). This effect explains the results obtained in winter, especially the opposite effect observed in winter for the GKDE (representative of eddy accumulation) and backward FTLE (more representative of accumulation at fronts and filaments) results.

This study contributes to widening our knowledge on the ocean dynamics mechanisms that affect surface transport. We have found that to better understand the global geometry of the oceanic flow (in terms of LCS and transport barriers), tides are needed. This opens the door to more studies to further analyze the tidal impacts on not only surface ocean transport, but also at depth and on the oceanic mixing properties. Furthermore, the impact of the fine-scales, and especially unbalanced motions like internal waves, on ocean surface dynamics is currently still being studied (Shakespeare & McC. Hogg, 2018; Thomas & Daniel, 2021; Gula et al., 2022). Future work could look further into this by analysing the impact of the different temporal and spatial scales on Lagrangian dynamics. In particular, the high-frequency motions due to tides, whose impact will be relevant with the novel ocean data from upcoming satellite missions like the Surface Water Ocean Topography satellite (Morrow et al., 2019).

In this study we were limited by the timespan of the eNATL60 simulation, so we were able to analyse data for only one year. It would be interesting to investigate the interannual variability of the tidal effects obtained as there is an EKE interannual variability in this region (Martins et al., 2002). When new model simulations allow it, it would be useful to reproduce this study over longer periods than the one-year outputs we were limited to here. Nevertheless, this twin simulation at a high resolution without and with tidal forcing is a unique dataset, and more scenarios can be explored. Our results are relevant to other regions, especially those with similar ocean dynamics, like high internal waves signal. In next studies the method applied here could be repeated in other regions to investigate if there are any differences in the magnitude and seasonality of the tidal impacts found here. Interesting regions would be ones with a lower internal waves signal (e.g., eastern part of the North Atlantic basin, or the Gulf Stream region) and with a higher impact of tidal currents (e.g. the North Sea).

Focusing on Lagrangian trajectory studies around archipelagos and coastal regions, it would be interesting to study the impact of tidal forcing on the arrival (Sala et al., 2016) and beaching (e.g. Yoon et al., 2010; Kaandorp et al., 2020) of virtual particles and the connectivity between islands (Vaz et al., 2013). It would also be interesting to study its impact on the surface-ocean connectivity timescales at a global scale (Jönsson & Watson, 2016). These have important impacts on the understanding of the biodiversity and pollution threats, especially on islands, and the consequent strategies necessary for their protection.

To conclude, we used a unique dataset to understand the effect of tides on ocean surface particle accumulation. This was the first time that Lagrangian ocean dynamics has been studied with a twin model without and with tidal forcing. We found that to better understand the global geometry of the flow (for example the presence of LCS and transport barriers), it is necessary not only to consider tidal forcing in OGCMs or data on tidal currents, but also their impact on other oceanic structures. This has important implications for Lagrangian simulations using OGCMs to study a range of topics, like for example, marine pollution (e.g. understanding the source of plastic pollution and the trajectory of an oil spill or of algae like *Sargassum*) and marine connectivity studies (e.g. of marine species via larvae dispersion). We shed some light on our understanding of the ocean by showing that tides play an important role in horizontal Lagrangian dynamics. This in turn affects not only our physical understanding of the ocean, but also of other biogeochemical and ecological processes in different parts of the global ocean.

Appendix A Backward FTLE distribution

The PDFs of the bFTLE fields for day 1 of each month are shown in fig. A1. All PDFs are positively skewed, demonstrating that the threshold of 0.5 $days^{-1}$ is representative of the start of the tail for all months.

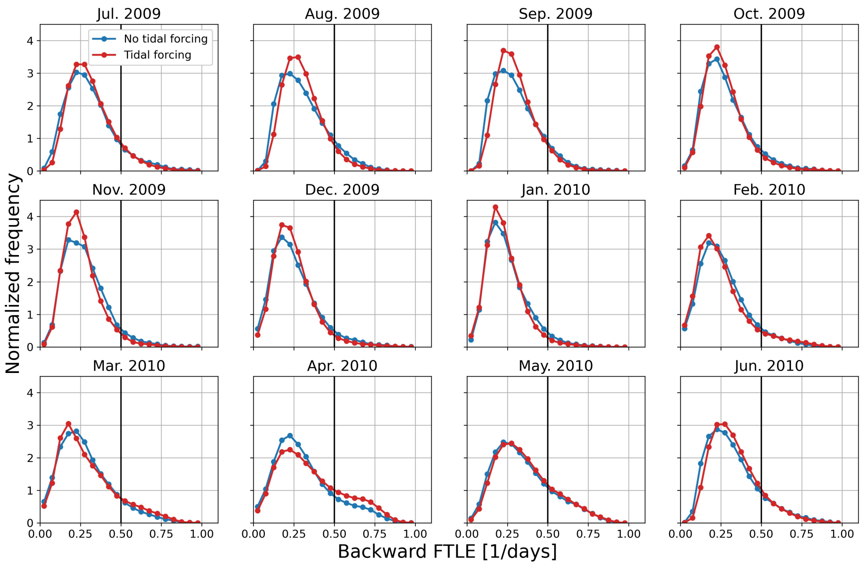

Figure A1. Probability density function of the backward FTLE fields on day 01 of each month for the no tidal forcing (blue) and tidal forcing (red) simulations. The vertical black line shows the threshold used at 0.5 $days^{-1}$.

Appendix B Open Research

Details on the model data used in this study, eNATL60, and its availability can be found here `https://github.com/ocean-next/eNATL60` (Brodeau et al., 2020a). The codes used to generate the Lagrangian simulations and analyse them can be found here: `https://github.com/OceanParcels/Azores_TidalForcing`.

Acknowledgments

LGN and EvS were partly funded by the European Research Council (ERC) under the European Union Horizon 2020 research and innovation programme (grant agreement No 715386) and the ESA World Ocean Circulation project, ESA Contract No. 4000130730/20/INB. EvS was also partly supported through the IMMERSE project from the European Union Horizon 2020 Research and Innovation Program (grant agreement no. 821926). VMM was supported by the MORHOC'H2 project, funded by the French "Agence Nationale de la Recherche" and "Direction Générale de l'Armement", grant number 21-ASM1-0003.

References

Ainsworth, C. H., Chassignet, E. P., French-McCay, D., Beegle-Krause, C. J., Berenshtein, I., Englehardt, J., ... Zheng, Y. (2021). Ten years of modeling the Deepwater Horizon oil spill. *Environmental Modelling & Software*, *142*, 105070. doi: 10.1016/j.envsoft.2021.105070

Ajayi, A., Le Sommer, J., Chassignet, E., Molines, J.-M., Xu, X., Albert, A., & Cosme, E. (2020). Spatial and Temporal Variability of the North Atlantic Eddy Field From Two Kilometric-Resolution Ocean Models. *Journal of Geophysical Research: Oceans*, *125*(5), e2019JC015827. doi: 10.1029/2019JC015827

Ansong, J. K., Arbic, B. K., Menemenlis, D., Wallcraft, A. J., Bourdalle-Badie, R., Chanut, J., ... others (2020). Importance of damping in comparison of internal tides in several global hydrodynamical models with altimetry. In *Ocean sciences meeting 2020.*

Arbic, B. K., Alford, M. H., Ansong, J. K., Buijsman, M. C., Ciotti, R. B., Farrar, J. T., ... others (2018). Primer on global internal tide and internal gravity wave continuum modeling in HYCOM and MITgcm. *New frontiers in operational oceanography*, 307–392.

Barkan, R., Srinivasan, K., Yang, L., McWilliams, J. C., Gula, J., & Vic, C. (2021). Oceanic Mesoscale Eddy Depletion Catalyzed by Internal Waves. *Geophysical Research Letters*, *48*(18), e2021GL094376. doi: 10.1029/2021GL094376

Barkan, R., Winters, K. B., & McWilliams, J. C. (2017). Stimulated imbalance and the enhancement of eddy kinetic energy dissipation by internal waves. *Journal of Physical Oceanography*, *47*(1), 181–198.

Bello-Fuentes, F. J., García-Nava, H., Andrade-Canto, F., Durazo, R., Castro, R., & Yarbuh, I. (2021). Tiempo de retención y capacidad de transporte de los remolinos del noroeste del golfo de México. *Ciencias Marinas*, *47*(2), 71–88. doi: 10.7773/cm.v47i2.3116

Beron-Vera, F. J., Olascoaga, M. J., & Goni, G. J. (2010). Surface Ocean Mixing Inferred from Different Multisatellite Altimetry Measurements. *Journal of Physical Oceanography*, *40*(11), 2466–2480. doi: 10.1175/2010JPO4458.1

Boffetta, G., Lacorata, G., Redaelli, G., & Vulpiani, A. (2001). Detecting barriers to transport: A review of different techniques. *Physica D: Nonlinear Phenomena*, *159*(1-2), 58–70. doi: 10.1016/S0167-2789(01)00330-X

Brodeau, L., Le Sommer, J., & Albert, A. (2020a). *eNATL60 dataset.* Retrieved from `https://github.com/ocean-next/eNATL60` doi: 10.5281/zenodo.4032732

Brodeau, L., Le Sommer, J., & Albert, A. (2020b). *eNATL60: Material describing the set-up and the assessment of NEMO-eNATL60 simulations.* Zenodo. Retrieved from `https://doi.org/10.5281/zenodo.4032732` doi: 10.5281/zenodo.4032732

Brunner, K., Kukulka, T., Proskurowski, G., & Law, K. L. (2015). Passive buoyant tracers in the ocean surface boundary layer: 2. observations and simulations of microplastic marine debris. *Journal of Geophysical Research: Oceans*, *120*(11), 7559–7573.

Bühler, O., & McIntyre, M. E. (2005). Wave capture and wave–vortex duality. *Journal of Fluid Mechanics*, *534*, 67–95.

Bôas, A. B., Ardhuin, F., Ayet, A., Bourassa, M. A., Brandt, P., Chapron, B., . . . Sebille, E. v. (2019). Integrated observations of global surface winds, currents, and waves: Requirements and challenges for the next decade. *Frontiers in Marine Science*, *6*, 425. doi: 10.3389/fmars.2019.00425

Cardoso, C., & Caldeira, R. M. A. (2021). Modeling the Exposure of the Macaronesia Islands (NE Atlantic) to Marine Plastic Pollution. *Frontiers in Marine Science*, *8*, 332. doi: 10.3389/fmars.2021.653502

Chamecki, M., Chor, T., Yang, D., & Meneveau, C. (2019). Material Transport in the Ocean Mixed Layer: Recent Developments Enabled by Large Eddy Simulations. *Reviews of Geophysics*, *57*(4), 1338–1371. doi: 10.1029/2019RG000655

Condie, S. A., & Condie, R. (2016). Retention of plankton within ocean eddies. *Global Ecology and Biogeography*. doi: 10.1111/geb.12485

Delandmeter, P., & van Sebille, E. (2019). The Parcels v2.0 Lagrangian framework: new field interpolation schemes. *Geoscientific Model Development*, *12*(8), 3571–3584. doi: 10.5194/gmd-12-3571-2019

Dobler, D., Huck, T., Maes, C., Grima, N., Blanke, B., Martinez, E., & Ardhuin, F. (2019). Large impact of Stokes drift on the fate of surface floating debris in the South Indian Basin. *Marine Pollution Bulletin*, *148*, 202–209. doi: 10.1016/j.marpolbul.2019.07.057

Drillet, Y., Chune, S. L., Levier, B., & Drevillon, M. (2019). Smoc: a new global surface current product containing the effect of the ocean general circulation, waves and tides. In *Geophysical research abstracts* (Vol. 21).

Díaz-Barroso, L., Hernández-Carrasco, I., Orfila, A., Reglero, P., Balbín, R., Hidalgo, M., … Alvarez-Berastegui, D. (2022). Singularities of surface mixing activity in the Western Mediterranean influence bluefin tuna larval habitats. *Marine Ecology Progress Series*, *685*, 69–84. doi: 10.3354/meps13979

d'Asaro, E. A., Shcherbina, A. Y., Klymak, J. M., Molemaker, J., Novelli, G., Guigand, C. M., … others (2018). Ocean convergence and the dispersion of flotsam. *Proceedings of the National Academy of Sciences*, *115*(6), 1162–1167.

d'Ovidio, F., Monte, S. D., Penna, A. D., Cotté, C., & Guinet, C. (2013). Ecological implications of eddy retention in the open ocean: a Lagrangian approach. *Journal of Physics A: Mathematical and Theoretical*, *46*(25), 254023. doi: 10.1088/1751-8113/46/25/254023

Gula, J., Taylor, J., Shcherbina, A., & Mahadevan, A. (2022). Chapter 8 - Submesoscale processes and mixing. In M. Meredith & A. Naveira Garabato (Eds.), *Ocean Mixing* (pp. 181–214). Elsevier. doi: 10.1016/B978-0-12-821512-8.00015

-3

Haller, G. (2001). Distinguished material surfaces and coherent structures in three-dimensional fluid flows. *Physica D: Nonlinear Phenomena*, *149*(4), 248–277. doi: 10.1016/S0167-2789(00)00199-8

Haller, G. (2015). Lagrangian Coherent Structures. *Annu. Rev. Fluid Mech*, *47*, 137–162. doi: 10.1146/annurev-fluid-010313-141322

Haller, G., & Yuan, G. (2000). Lagrangian coherent structures and mixing in two-dimensional turbulence. *Physica D: Nonlinear Phenomena*, *147*(3-4), 352–370.

Haza, A. C., Özgökmen, T. M., & Hogan, P. (2016). Impact of submesoscales on surface material distribution in a gulf of Mexico mesoscale eddy. *Ocean Modelling*, *107*, 28–47. doi: 10.1016/j.ocemod.2016.10.002

Hernández-Carrasco, I., Alou-Font, E., Dumont, P.-A., Cabornero, A., Allen, J., & Orfila, A. (2020). Lagrangian flow effects on phytoplankton abundance and composition along filament-like structures. *Progress in Oceanography*, *189*, 102469. doi: 10.1016/j.pocean.2020.102469

Hernández-Carrasco, I., López, C., Hernández-García, E., & Turiel, A. (2011). How reliable are finite-size Lyapunov exponents for the assessment of ocean dynamics? *Ocean Modelling*, *36*(3-4), 208–218. doi: 10.1016/j.ocemod.2010.12.006

Hernández-Carrasco, I., Orfila, A., Rossi, V., & Garçon, V. (2018). Effect of small scale transport processes on phytoplankton distribution in coastal seas. *Scientific Reports*, *8*(1), 8613. doi: 10.1038/s41598-018-26857-9

Hidalgo, M., Rossi, V., Monroy, P., Ser-Giacomi, E., Hernández-García, E., Guijarro, B., … Reglero, P. (2019). Accounting for ocean connectivity and hydroclimate in fish recruitment fluctuations within transboundary metapopulations. *Ecological Applications*, *29*(5), e01913. doi: 10.1002/eap.1913

Higgins, C., Vanneste, J., & Bremer, T. S. (2020). Unsteady Ekman-Stokes Dynamics: Implications for Surface Wave-Induced Drift of Floating Marine Litter. *Geophysical Research Letters*, *47*(18), e2020GL089189. doi: 10.1029/2020GL089189

Huntley, H. S., Lipphardt Jr., B. L., Jacobs, G., & Kirwan Jr., A. D. (2015). Clusters, deformation, and dilation: Diagnostics for material accumulation regions. *Journal of Geophysical Research: Oceans*, *120*(10), 6622–6636. doi: 10.1002/2015JC011036

Iwasaki, S., Isobe, A., Kako, S., Uchida, K., & Tokai, T. (2017). Fate of microplastics and mesoplastics carried by surface currents and wind waves: A numerical model approach in the Sea of Japan. *Marine Pollution Bulletin*, *121*(1), 85–96. doi: 10.1016/j.marpolbul.2017.05.057

Jackson, C. R. (2004). *An atlas of internal solitary-like waves and their properties.* Retrieved from `http://www.internalwaveatlas.com/Atlas2_index.html`

Jackson, C. R., da Silva, J., & Jeans, G. (2012). The Generation of nonlinear internal waves. *Oceanography*, *25*(2), 108–123. doi: 10.5670/oceanog.2012.46

Jönsson, B. F., & Watson, J. R. (2016). The timescales of global surface-ocean connectivity. *Nature Communications*, *7*(1), 11239. doi: 10.1038/ncomms11239

Kaandorp, M. L., Dijkstra, H. A., & van Sebille, E. (2020). Closing the Mediterranean Marine Floating Plastic Mass Budget: Inverse Modeling of Sources and Sinks. *Environmental Science and Technology*, *54*(19), 11980–11989. doi: 10.1021/acs.est.0c01984

Krüger, L., Ramos, J., Xavier, J., Grémillet, D., González-Solís, J., Kolbeinsson, Y., … others (2017). Identification of candidate pelagic marine protected areas through a seabird seasonal-, multispecific-and extinction risk-based approach. *Animal Conservation*, *20*(5), 409–424.

Lahaye, N., Gula, J., & Roullet, G. (2019). Sea Surface Signature of Internal Tides. *Geophysical Research Letters*, *46*(7), 3880–3890. doi: 10.1029/2018GL081848

Largier, J. L. (2003). Considerations in Estimating Larval Dispersal Distances from Oceanographic Data. *Ecological Applications*, *13*(sp1), 71–89. doi: 10.1890/1051-0761(2003)013[0071:CIELDD]2.0.CO;2

Le Sommer, J., Chassignet, E. P., & Wallcraft, A. J. (2018). Ocean Circulation Modeling for Operational Oceanography: Current Status and Future Challenges. *New frontiers in operational oceanography*, 289–306. doi: 10.17125/gov2018.ch12.289

Lévy, M., Ferrari, R., Franks, P. J., Martin, A. P., & Rivière, P. (2012). Bringing physics to life at the submesoscale. *Geophysical Research Letters*, *39*(14).

Lévy, M., Klein, P., & Treguier, A.-M. (2001). Impact of sub-mesoscale physics on production and subduction of phytoplankton in an oligotrophic regime. *Journal of marine research*, *59*(4), 535–565.

Limer, B. D., Bloomberg, J., & Holstein, D. M. (2020). The influence of eddies on coral larval retention in the flower garden banks. *Frontiers in Marine Science*. doi: 10.3389/fmars.2020.00372

Lin, L., von Storch, H., Chen, X., Jiang, W., & Tang, S. (2023). Link between the internal variability and the baroclinic instability in the bohai and yellow sea. *Ocean Dynamics*, 1–14. doi: 10.1007/s10236-023-01583-7

Liu, Y., Weisberg, R. H., Vignudelli, S., & Mitchum, G. T. (2014). Evaluation of altimetry-derived surface current products using Lagrangian drifter trajectories in the eastern Gulf of Mexico. *Journal of Geophysical Research: Oceans*, *119*(5), 2827–2842. doi: 10.1002/2013JC009710

Mahadevan, A. (2016). The impact of submesoscale physics on primary productivity of plankton. *Annual review of marine science*, *8*, 161–184.

Martins, C. S., Hamann, M., & Fiúza, A. F. G. (2002). Surface circulation in the eastern North Atlantic, from drifters and altimetry. *Journal of Geophysical Research: Oceans*, *107*(C12), 10–1–10–22. doi: 10.1029/2000JC000345

Maximenko, N., Hafner, J., Kamachi, M., & MacFadyen, A. (2018). Numerical simulations of debris drift from the Great Japan Tsunami of 2011 and their verification with observational reports. *Marine Pollution Bulletin*, *132*, 5–25. doi: 10.1016/j.marpolbul.2018.03.056

Maximenko, N., Hafner, J., & Niiler, P. (2012). Pathways of marine debris derived from trajectories of Lagrangian drifters. *Marine Pollution Bulletin*, *65*. doi: 10.1016/j.marpolbul.2011.04.016

McWilliams, J. C., Gula, J., & Molemaker, M. J. (2019). The gulf stream north wall: Ageostrophic circulation and frontogenesis. *Journal of Physical Oceanography*, *49*(4), 893–916.

Miron, P., Olascoaga, M. J., Beron-Vera, F. J., Putman, N. F., Triñanes, J., Lumpkin, R., & Goni, G. J. (2020). Clustering of Marine-Debris- and *Sargassum*-Like Drifters Explained by Inertial Particle Dynamics. *Geophysical Research Letters*, *47*(19). doi: 10.1029/2020GL089874

Morales-Márquez, V., Hernández-Carrasco, I., Fox-Kemper, B., & Orfila, A. (2023). Ageostrophic contribution by the wind and waves induced flow to the lateral stirring in the mediterranean sea. *Journal of Geophysical Research: Oceans*, *128*(4), e2022JC019135. doi: 10.1029/2022JC019135

Morales-Márquez, V., Hernández-Carrasco, I., Simarro, G., Rossi, V., & Orfila, A.

(2021). Regionalizing the Impacts of Wind- and Wave-Induced Currents on Surface Ocean Dynamics: A Long-Term Variability Analysis in the Mediterranean Sea. *Journal of Geophysical Research: Oceans*, *126*(9), e2020JC017104. doi: 10.1029/2020JC017104

Morrow, R., Fu, L.-L., Ardhuin, F., Benkiran, M., Chapron, B., Cosme, E., … Zaron, E. D. (2019). Global Observations of Fine-Scale Ocean Surface Topography With the Surface Water and Ocean Topography (SWOT) Mission. *Frontiers in Marine Science*, *6*, 232. doi: 10.3389/fmars.2019.00232

Mtfller, P. (1976). On the diffusion of momentum and mass by internal gravity waves. *Journal of Fluid Mechanics*, *77*(4), 789–823. doi: 10.1017/S0022112076002899

Onink, V., Wichmann, D., Delandmeter, P., & van Sebille, E. (2019). The role of ekman currents, geostrophy, and stokes drift in the accumulation of floating microplastic. *Journal of Geophysical Research: Oceans*, *124*(3), 1474–1490.

Pham, C. K., Pereira, J. M., Frias, J. P. G. L., Ríos, N., Carriço, R., Juliano, M., & Rodríguez, Y. (2020). Beaches of the Azores archipelago as transitory repositories for small plastic fragments floating in the North-East Atlantic. *Environmental Pollution*, *263*, 114494. doi: 10.1016/j.envpol.2020.114494

Poje, A. C., Özgökmen, T. M., Lipphardt Jr, B. L., Haus, B. K., Ryan, E. H., Haza, A. C., … others (2014). Submesoscale dispersion in the vicinity of the deepwater horizon spill. *Proceedings of the National Academy of Sciences*, *111*(35), 12693–12698. doi: 10.1073/pnas.140245211

Putman, N. F., Lumpkin, R., Olascoaga, M. J., Trinanes, J., & Goni, G. J. (2020). Improving transport predictions of pelagic Sargassum. *Journal of Experimental Marine Biology and Ecology*, *529*, 151398. doi: 10.1016/j.jembe.2020.151398

Ray, R. D., & Zaron, E. D. (2016). M2 Internal Tides and Their Observed Wavenumber Spectra from Satellite Altimetry. *Journal of Physical Oceanograph*, *46*(1), 3–22. doi: 10.1175/JPO-D-15-0065.1

Rocha, C. B., Gille, S. T., Chereskin, T. K., & Menemenlis, D. (2016). Seasonality of submesoscale dynamics in the Kuroshio Extension. *Geophysical Research Letters*, *43*(21), 11–304. doi: 10.1002/2016GL071349

Révelard, A., Reyes, E., Mourre, B., Hernández-Carrasco, I., Rubio, A., Lorente, P., … Tintoré, J. (2021). Sensitivity of Skill Score Metric to Validate Lagrangian

Simulations in Coastal Areas: Recommendations for Search and Rescue Applications. *Frontiers in Marine Science*, *8*, 191. doi: 10.3389/fmars.2021.630388

Sala, I., Harrison, C. S., & Caldeira, R. M. (2016). The role of the azores archipelago in capturing and retaining incoming particles. *Journal of Marine Systems*, *154*, 146-156. doi: 10.1016/j.jmarsys.2015.10.001

Savage, A. C., Arbic, B. K., Richman, J. G., Shriver, J. F., Alford, M. H., Buijsman, M. C., ... others (2017). Frequency content of sea surface height variability from internal gravity waves to mesoscale eddies. *Journal of Geophysical Research : Oceans*, *122*(3), 2519–2538.

Scott, D. W. (1992). *Multivariate density estimation: theory, practice, and visualization.* John Wiley & Sons Inc., New York, USA. doi: 10.1002/9780470316849

Shadden, S. C., Lekien, F., & Marsden, J. E. (2005). Definition and properties of Lagrangian coherent structures from finite-time Lyapunov exponents in two-dimensional aperiodic flows. *Physica D: Nonlinear Phenomena*, *212*(3-4), 271–304. doi: 10.1016/j.physd.2005.10.007

Shakespeare, C. J., & McC. Hogg, A. (2018). The Life Cycle of Spontaneously Generated Internal Waves. *Journal of Physical Oceanography*, *48*(2). doi: 10.1175/JPO-D-17-0153.1

Shanks, A. L. (2021). Observational evidence and open questions on the role of internal tidal waves on the concentration and transport of floating plastic debris. *Frontiers in Marine Science*, *8*, 633. doi: 10.3389/fmars.2021.621062

Stammer, D. (1997). Global characteristics of ocean variability estimated from regional TOPEX/ POSEIDON altimeter measurements. *Journal of Physical Oceanography*, *27*, 1743-1769. doi: 10.1175/1520-0485(1997)027⟨1743:GCOOVE⟩2.0.CO;2

Sterl, M. F., Delandmeter, P., & van Sebille, E. (2020). Influence of barotropic tidal currents on transport and accumulation of floating microplastics in the global open ocean. *Journal of Geophysical Research: Oceans*, *125*(2), e2019JC015583.

Sutherland, B. R., & Yassin, H. (2022). The nonlinear evolution of internal tides. Part 2. Lagrangian transport by periodic and modulated waves. *Journal of Fluid Mechanics*, *948*, A22. doi: 10.1017/jfm.2022.690

Tarry, D. R., Essink, S., Pascual, A., Ruiz, S., Poulain, P.-M., Özgökmen, T.,

... others (2021). Frontal convergence and vertical velocity measured by drifters in the alboran sea. *Journal of Geophysical Research: Oceans*, *126*(4), e2020JC016614.

Thomas, J., & Daniel, D. (2021). Forward flux and enhanced dissipation of geostrophic balanced energy. *Journal of Fluid Mechanics*, *911*. doi: 10.1017/jfm.2020.1026

Torres, H. S., Klein, P., Menemenlis, D., Qiu, B., Su, Z., Wang, J., ... Fu, L.-L. (2018). Partitioning Ocean Motions Into Balanced Motions and Internal Gravity Waves: A Modeling Study in Anticipation of Future Space Missions. *Journal of Geophysical Research: Oceans*, *123*(11), 8084–8105. doi: 10.1029/2018JC014438

Tsiaras, K., Hatzonikolakis, Y., Kalaroni, S., Pollani, A., & Triantafyllou, G. (2021). Modeling the Pathways and Accumulation Patterns of Micro- and Macro-Plastics in the Mediterranean. *Frontiers in Marine Science*, *8*, 1389. doi: 10.3389/fmars.2021.743117

van Sebille, E., Aliani, S., Law, K. L., Maximenko, N., Alsina, J. M., Bagaev, A., ... others (2020). The physical oceanography of the transport of floating marine debris. *Environmental Research Letters*, *15*(2), 023003.

van Sebille, E., England, M. H., & Froyland, G. (2012). Origin, dynamics and evolution of ocean garbage patches from observed surface drifters. *Environmental Research Letters*, *7*(4), 044040. doi: 10.1088/1748-9326/7/4/044040

van Sebille, E., Zettler, E., Wienders, N., Amaral-Zettler, L., Elipot, S., & Lumpkin, R. (2021). Dispersion of surface drifters in the tropical atlantic. *Frontiers in Marine Science*, *7*, 1243. doi: 10.3389/fmars.2020.607426

Vaz, A. C., Richards, K. J., Jia, Y., & Paris, C. B. (2013). Mesoscale flow variability and its impact on connectivity for the island of Hawai'i. *Geophysical Research Letters*, *40*(2), 332–337. doi: 10.1029/2012GL054519

Verron, J., Bonnefond, P., Andersen, O., Ardhuin, F., Bergé-Nguyen, M., Bhowmick, S., ... Zaron, E. (2020). The SARAL / AltiKa mission : A step forward to the future of altimetry. *Advances in Space Research*. doi: 10.1016/j.asr.2020.01.030

Wenegrat, J. O., & McPhaden, M. J. (2016). Wind, Waves, and Fronts: Frictional Effects in a Generalized Ekman Model. *Journal of Physical Oceanography*, *46*(2), 371–394. doi: 10.1175/JPO-D-15-0162.1

White, G. H. (1980). Skewness, Kurtosis and Extreme Values of Northern Hemisphere Geopotential Heights. *Monthly Weather Review*, *108*(9), 1446–1455. doi: 10.1175/1520-0493(1980)108⟨1446:SKAEVO⟩2.0.CO;2

Yoon, J.-H., Kawano, S., & Igawa, S. (2010). Modeling of marine litter drift and beaching in the Japan Sea. *Marine Pollution Bulletin*, *60*(3), 448–463. doi: 10.1016/j.marpolbul.2009.09.033